Neuron

Article

The Loss of TBK1 Kinase Activity in Motor Neurons or in All Cell Types Differentially Impacts ALS Disease Progression in SOD1 Mice

Graphical Abstract

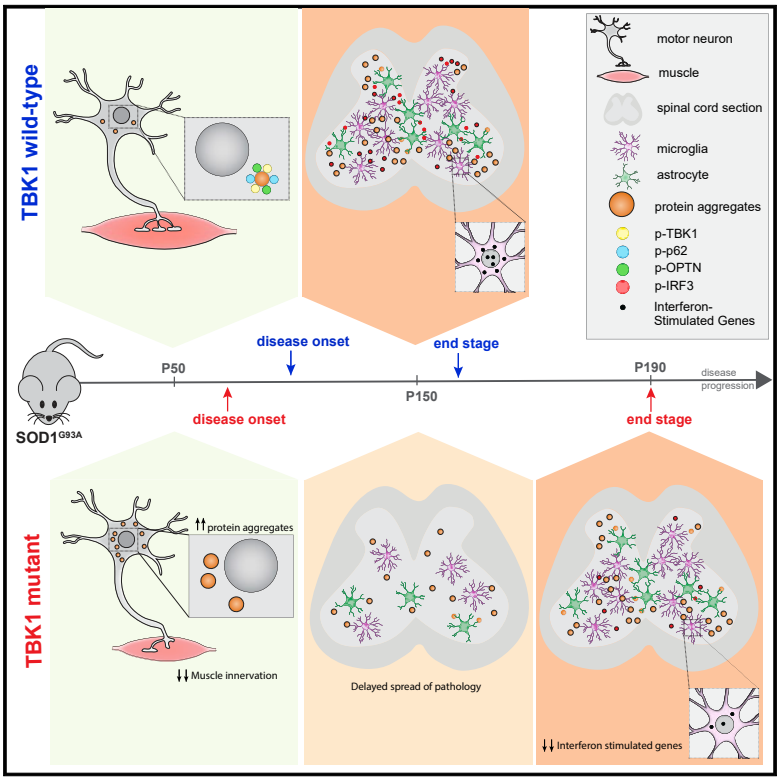

Highlights

- TBK1 kinase activity regulates disease progression in an ALS SOD1 mouse model
- Loss of TBK1 in motor neurons increases SOD1 aggregation and accelerates disease onset
- Loss of TBK1 activity in all cell types accelerates disease onset but extends survival
- Loss of TBK1 activity in all cell types reduces the IFN response in microglia

Authors

Valeria Gerbino, Esther Kaunga, Junqiang Ye, ..., Paolo Guarnieri, Cathleen M. Lutz, Tom Maniatis

Correspondence

tm2472@columbia.edu

In Brief

DNA sequence variants in the *TBK1* gene associate with familial and sporadic ALS. Gerbino et al. show that partial or complete loss-of-function TBK1 mutations alone do not induce neurodegeneration in mice. However, they profoundly affect disease onset and progression in the SOD1 ALS mouse model.

Gerbino et al., 2020, Neuron *106*, 789–805
June 3, 2020
https://doi.org/10.1016/j.neuron.2020.03.005

CellPress

Neuron

CellPress

Article

The Loss of TBK1 Kinase Activity in Motor Neurons or in All Cell Types Differentially Impacts ALS Disease Progression in SOD1 Mice

Valeria Gerbino,[1,2] Esther Kaunga,[1,2] Junqiang Ye,[1,2] Daniele Canzio,[1,2] Sean O'Keeffe,[1] Noam D. Rudnick,[1] Paolo Guarnieri,[1,3] Cathleen M. Lutz,[4] and Tom Maniatis[1,2,5,6,7,*]

[1]Department of Biochemistry and Molecular Biophysics, Columbia University, New York, NY 10032, USA
[2]Mortimer B. Zuckerman Mind Brain and Behavior Institute, Columbia University, New York, NY 10027, USA
[3]Department of Systems Biology, Columbia University, New York, NY 10032, USA
[4]The Jackson Laboratory, 600 Main Street, Bar Harbor, ME 04609, USA
[5]New York Genome Center, New York, NY 10013, USA
[6]Vagelos College of Physicians and Surgeons, Columbia University, New York, NY 10032, USA
[7]Lead contact
*Correspondence: tm2472@columbia.edu
https://doi.org/10.1016/j.neuron.2020.03.005

SUMMARY

DNA sequence variants in the *TBK1* gene associate with or cause sporadic or familial amyotrophic lateral sclerosis (ALS). Here we show that mice bearing human ALS-associated TBK1 missense loss-of-function mutations, or mice in which the *Tbk1* gene is selectively deleted in motor neurons, do not display a neurodegenerative disease phenotype. However, loss of TBK1 function in motor neurons of the SOD1^{G93A} mouse model of ALS impairs autophagy, increases SOD1 aggregation, and accelerates early disease onset without affecting lifespan. By contrast, point mutations that decrease TBK1 kinase activity in all cells also accelerate disease onset but extend the lifespan of SOD1 mice. This difference correlates with the failure to activate high levels of expression of interferon-inducible genes in glia. We conclude that loss of TBK1 kinase activity impacts ALS disease progression through distinct pathways in different spinal cord cell types and further implicate the importance of glia in neurodegeneration.

INTRODUCTION

Amyotrophic lateral sclerosis (ALS) is a fatal neurodegenerative disease characterized by motor neuron loss, neuromuscular denervation, and progressive paralysis. Although cell-autonomous mechanisms in motor neurons are central to ALS pathology, many non-cell-autonomous contributions to disease onset and progression have been identified, originating from microglia, astrocytes, and oligodendrocytes (Taylor et al., 2016). Accumulation of misfolded proteins in cytoplasmic inclusions is a common feature of both sporadic and familial ALS and other neurodegenerative diseases (Blokhuis et al., 2013). Other cellular abnormalities in ALS include mitochondrial vacuolization, fragmentation of the Golgi apparatus, and abnormal neuromuscular junctions (Blokhuis et al., 2013). In addition, the spread of protein aggregates and neuroinflammation through the spinal cord and brain is a hallmark of disease progression in ALS (Taylor et al., 2016). Pathology-associated protein aggregates and damaged cellular organelles are targeted to the ubiquitin-proteasome pathway and the autophagy system for clearance. An important role of autophagy in ALS was revealed by large-scale whole-exome sequencing and genome-wide association studies (GWAS) studies, which identified DNA sequence variants in several autophagy pathway genes in ALS patients, including VCP, UBQLN2, CHMP2B, p62, OPTN, C9orf72, and TANK-Binding Kinase 1 (TBK1) (Oakes et al., 2017; Taylor et al., 2016).

In previous studies we investigated the role of autophagy in ALS by conditionally deleting the essential autophagy gene *Atg7* from cholinergic neurons in the SOD1^{G93A} mouse model of ALS (Rudnick et al., 2017). We found that the loss of autophagy in motor neurons accelerates the denervation of neuromuscular junctions in early stages of the disease but diminishes the spread of pathology to other cell types late in disease, thus reducing neuroinflammation in a non-cell-autonomous manner (Rudnick et al., 2017).

Neuroinflammation is a prominent feature in postmortem ALS patient samples and in mutant SOD1 transgenic mouse models of ALS (Taylor et al., 2016) and is characterized by the activation of microglia and astrocytes, as well as inflammatory pathways that contribute to progressive neurodegeneration (Geloso et al., 2017). In addition, genetic approaches in mouse models have revealed an important role for astrocytes and microglia in driving neurodegeneration (Boillée et al., 2006; Clement et al., 2003; Yamanaka et al., 2008). All these studies have shown that the accumulation of misfolded protein aggregates, autophagy, and neuroinflammation play important roles in the ALS disease process. A detailed understanding of the regulatory mechanisms that underlie these activities and their interplay is crucial to better understand ALS disease mechanisms.

TBK1, which plays an important regulatory role in autophagy, innate immunity, neuroinflammation, and apoptosis (Oakes et al., 2017; Xu et al., 2018), was identified as an ALS gene in large-scale

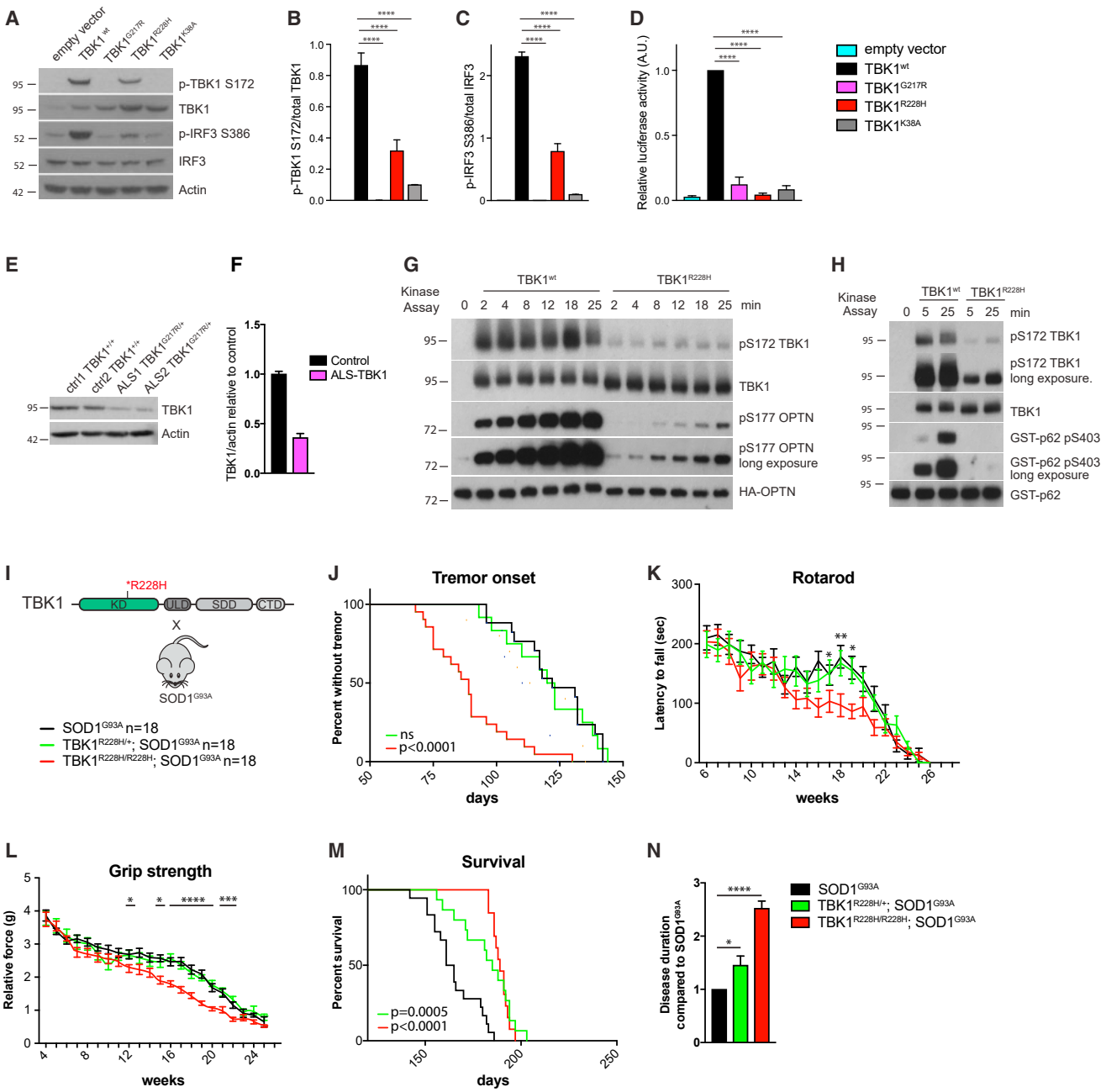

Figure 1. The TBK1 R228H Mutation Leads to Partial Loss of Kinase Function and Alters ALS Disease Progression in SOD1^{G93A} Mice

(A–C) Western blot (A) and relative band densitometry of protein lysates from HEK293T cells transfected with the indicated constructs show that TBK1 G217R and R228H mutations completely or partially (respectively) reduce autophosphorylation (B) and kinase activity toward the transcription factor IRF3 (C).

(D) Interferon-β promoter luciferase assay shows reduced ability of TBK1 G217R and R228H mutants to activate the Interferon-β promoter.

(E and F) Western blot (E) and relative band densitometry (F) of protein lysates from fibroblasts of ALS patients carrying the TBK1 G217R mutation show that TBK1 protein levels are lower compared to healthy controls.

(G and H) Kinase assays show that TBK1 R228H is less effective than TBK1 WT in phosphorylating the autophagy receptors optineurin (G) and p62 (H).

(I) Generation of TBK1 mutant SOD1^{G93A} mice. The position of the R228H mutation in the kinase domain of the TBK1 gene is shown (KD, kinase domain; ULD, ubiquitin-like domain; SDD, scaffold dimerization domain; CTD; C-terminal domain). Different colors designate different genotypes.

(J) Kaplan-Meier plot showing effects of the TBK1 R228H mutation on disease onset. TBK1$^{R228H/R228H}$; SOD1^{G93A} Log-rank test = 27.35, $p < 0.0001$; TBK1$^{R228H/+}$; SOD1^{G93A} Log-rank test = 0.269, $p = 0.6$.

(K and L) TBK1$^{R228H/R228H}$; SOD1^{G93A} but not TBK1$^{R228H/+}$; SOD1^{G93A} mice showed reduced performance on the rotarod (K) and grip strength force assay (L). Results are shown as mean ± SEM; *p = 0.0332, **p = 0.0021, ***p = 0.0002, ****p < 0.0001; multiple t tests.

(legend continued on next page)

whole-exome sequencing studies of sporadic and genetic studies of familial ALS, respectively (Cirulli et al., 2015; Freischmidt et al., 2015). TBK1 plays a central role in the cellular innate immune response, in particular the induction of type-I interferon gene expression, mainly through phosphorylation of IRF3/7 transcription factors (Fitzgerald et al., 2003; McWhirter et al., 2004; Sharma et al., 2003; Solis et al., 2007), and in selective autophagy. Specifically, TBK1-mediated phosphorylation of autophagy receptors enhances their binding to autophagosomal proteins and/or to ubiquitin, thus facilitating the clearance of protein aggregates and damaged mitochondria (Heo et al., 2015; Lazarou et al., 2015; Matsumoto et al., 2015; Moore and Holzbaur, 2016; Richter et al., 2016; Wild et al., 2011). Heterozygous TBK1 frameshift, splice-site, nonsense, missense, and deletion mutations associate with sporadic and familial ALS cases (reviewed in Oakes et al., 2017). Nonsense and frameshift mutations may act through a hemizygous loss of function mechanism. However, TBK1 functions as a dimer. Therefore, missense mutations and single amino acid deletions could also act through a complete or partial loss of function or a dominant negative mechanism.

Similar to our previous study of the role of the *Atg7* gene and autophagy in ALS disease progression (Rudnick et al., 2017), the role of TBK1 was studied using the SOD1 mouse model. Specifically, the effect of TBK1 haploinsufficiency was studied by global heterozygous deletion of TBK1 in SOD1^{G93A} mice (Brenner et al., 2019). This led to a modest acceleration of disease onset, denervation of neuromuscular junctions with no effect on motor neuron survival, and an impact on gliosis (Brenner et al., 2019). In particular it was proposed that TBK1 haploinsufficiency modulates the contribution of microglia to inflammation (Brenner et al., 2019). Although that study builds upon genetic evidence implicating a role for TBK1 in ALS, a heterozygous deletion may not faithfully model the human cases in which one of the two TBK1 alleles bears a missense mutation. In addition, given that the kinase activity of TBK1 is essential for its pleiotropic functions, the requirement of this activity for ALS disease onset and progression is critical to understanding the role of TBK1 in ALS.

Here we generate and characterize two different mouse strains, each bearing a distinct human ALS-associated point mutation which either diminishes or abolishes TBK1 kinase activity. We also examine the phenotypes of mice in which TBK1 is conditionally deleted in motor neurons, the vulnerable ALS cells, and thus provide insights into the cell-autonomous effects of TBK1 loss of function. We find that TBK1 kinase activity is required in the spinal cord of ALS mice for the phosphorylation of distinct downstream targets in specific cell types, and that TBK1 loss of function in motor neurons or other spinal cord cells differentially affects autophagy or the interferon response. These studies provide mechanistic insights into how TBK1 kinase activity can modify neurodegenerative disease onset and progression and reveal the complexity of the underlying genetic interactions.

RESULTS

Generation of Knockin TBK1 Mice Bearing Missense ALS Mutations

Over 90 distinct TBK1 DNA sequence variants associate with familial or sporadic ALS in genetic studies (Oakes et al., 2017). Among these are single nucleotide substitutions in the kinase domain. We recently reported a detailed study of the activities and dimerization properties of 25 of these substitutions (Ye et al., 2019). To establish animal models of TBK1-associated ALS, the missense mutations G217R (familial ALS) or R228H (associated with sporadic ALS) in the *Tbk1* gene were separately introduced into C57BL/6J mice by CRISPR mutagenesis as described in STAR Methods. Both single nucleotide mutations occur in the kinase domain of TBK1 and were chosen for *in vivo* studies based on results from biochemical assays (Figures 1A–1H). Similar to other studies (de Majo et al., 2018; Ye et al., 2019), when TBK1 G217R was expressed in HEK293T cells, autophosphorylation of serine 172 (S172) was not observed, consistent with a complete loss of kinase activity. By contrast, TBK1R228H displayed partial autophosphorylation and significantly reduced kinase activity toward TBK1 substrates such as IRF3, Optineurin (OPTN), and p62 (Figures 1A–1H).

While a neurodegenerative disease phenotype was not observed in heterozygous G217R mice, homozygous mutant mice were nonviable (Figure S1B), consistent with the phenotype of homozygous TBK1 deletion mice (Bonnard et al., 2000). However, like homozygous TBK1 KO mice (Bonnard et al., 2000), lethality of the homozygous TBK1 G217R mice can be rescued by a homozygous deletion of the TNF receptor gene (Figure S1C). Thus, the homozygous G217R mutation behaves as a complete loss-of-function mutation *in vitro* and *in vivo*. Western blots of protein lysates from TBK1$^{G217R/G217R}$; TNFR$^{-/-}$ mouse brains revealed that the mutant TBK1 G217R protein is expressed at low levels *in vivo* (Figure S1D), consistent with the reduced TBK1 protein levels observed in TBK1 G217R patient fibroblasts (Figures 1E and 1F). In contrast, homozygous R228H mice are born at the expected Mendelian ratios (Figure S1F), and the mutant TBK1 protein is stable *in vivo* (Figure S1G). Although heterozygous TBK1 loss-of-function mutations in humans associate with ALS, heterozygous TBK1 G217R mice, as well as homozygous and heterozygous TBK1 R228H mice, are viable and do not show overt motor defects. Quantification of spinal cord motor neurons and innervation of neuromuscular junctions (NMJs) at the ALS vulnerable tibialis anterior muscle revealed no difference with wild-type (WT) littermates up to 2 years of age (Figures S1H and S1I). Morphology analysis revealed fragmentation of NMJs typical of aging mice (Valdez et al., 2010), which was not affected by TBK1 mutations (Figures S1J and S1K).

TBK1 G217R and R228H Mutations Accelerate Disease Onset in SOD1^{G93A} Mice

An alternative approach to generating mouse models to study ALS disease was suggested by studies of the effects of genetic

(M) TBK1 R228H mutation extends the lifespan of SOD1 mice. TBK1$^{R228H/R228H}$; SOD1^{G93A} Log-rank test = 26.88, $p < 0.0001$; TBK1$^{R228H/+}$; SOD1^{G93A} Log-rank test = 12.31, $p = 0.0005$.

(N) Disease duration is extended by 1.4-fold in TBK1$^{R228H/+}$; SOD1^{G93A} and by 2.7-fold in TBK1$^{R228H/R228H}$; SOD1^{G93A} compared to SOD1^{G93A} mice. n = 18 animals per genotype, 9 males and 9 females.

variability in inbred mouse lines on disease progression of SOD1^{G93A} mice (Heiman-Patterson et al., 2011). Due to the lack of an overt neurodegenerative phenotype in the TBK1 mutant knockin mice, we crossed TBK1 G217R and TBK1 R228H mutant mice with SOD1^{G93A} transgenic mice to determine whether ALS-associated mutations in TBK1 affect disease progression in this ALS mouse model (Figures 1I and S2A).

To assess the specific contribution of TBK1 to disease progression, we also included in this study the loss of IKKε, a closely related kinase that shares protein substrates with TBK1 (Fitzgerald et al., 2003), addressing the possibility that the two kinases affect overlapping or redundant pathways that could contribute to neurodegeneration. With respect to TBK1, we observed a substantial (24.5%) acceleration of the onset of hind limb tremor in TBK1$^{R228H/R228H}$; SOD1^{G93A} mice (Figure 1J; median onset was 126.5 days in SOD1^{G93A} versus 89 days in TBK1$^{R228H/R228H}$; SOD1^{G93A} mice). By contrast, the heterozygous TBK1 R228H mutation did not alter disease onset (median disease onset for TBK1$^{R228H/+}$; SOD1^{G93A} was 123 days), thus revealing a clear dosage effect on disease onset. Notably, when subjected to motor function tests such as rotarod and grip strength force assays, TBK1$^{R228H/R228H}$; SOD1^{G93A} mice (but not TBK1$^{R228H/+}$; SOD1^{G93A} mice) displayed a significant exacerbation of the motor deficits (Figures 1K and 1L). Surprisingly, however, the TBK1 R228H allele (either heterozygous or homozygous) extended the survival of SOD1 mice by 13% and 16%, respectively (Figure 1M; median survival was 163 days for SOD1^{G93A} versus 185 days in TBK1$^{R228H/+}$; SOD1^{G93A} mice and 189 days in TBK1$^{R228H/R228H}$; SOD1^{G93A} mice). Thus, the TBK1 R228H mutation resulted in a significant increase in disease duration (time elapsed from disease onset to disease end stage). The increase was greater in homozygous mice, where disease duration was increased by 2.7-fold, while in heterozygous mice disease duration was increased by 1.4-fold compared to SOD1^{G93A} mice (Figure 1N).

The TBK1 familial G217R heterozygous mutation similarly affected disease onset and survival of SOD1^{G93A} mice (Figures S2B and S2D; median disease onset for TBK1$^{G217R/+}$; SOD1^{G93A} was 103 days and median survival was 180 days), resulting in a 1.8-fold increase in disease duration (Figure S2D). By contrast, homozygous deletion of IKKε had no effect on disease onset, survival, disease duration, or motor performance of SOD1 mice (Figures S2E–S2J). Thus, although IKKε and TBK1 share a subset of protein substrates, the loss of kinase activity of IKKε has no apparent effect on neurodegenerative disease progression in SOD1 mice. We conclude that reduced or abolished TBK1 kinase activity profoundly affects both early and late disease progression in the SOD1^{G93A} ALS mouse model.

Uncoupling NMJ Denervation from Motor Neuron Death in TBK1 R228H; SOD1^{G93A} Mice

NMJ degeneration typically precedes motor neuron loss and appearance of motor symptoms in the SOD1^{G93A} mouse model and can therefore serve as a sensitive anatomical correlate of disease. To determine the effects of the TBK1 R228H mutation on muscle innervation of SOD1 mice, we visualized innervation of the NMJs at the ALS-vulnerable fast tibialis anterior (TA) muscle. Consistent with the observed reduction in motor performance of TBK1$^{R228H/R228H}$; SOD1^{G93A} compared to SOD1^{G93A} mice, we found that the denervation of NMJs occurred earlier in mutant mice compared to mice with normal levels of TBK1 expression. Specifically, at postnatal day (P) 50, TBK1$^{R228H/R228H}$; SOD1^{G93A} mice showed 44.33% innervated NMJs compared to 64.17% in SOD1^{G93A} littermates (Figures 2A and 2B). However, at P100, TBK1$^{R228H/R228H}$; SOD1^{G93A} and SOD1^{G93A} mice showed similar levels of NMJ innervation at the TA (31.8% and 34.73%, respectively), revealing a reduced rate of NMJ denervation in TBK1 mutant mice at later stages of the disease.

Unexpectedly, the mutant TBK1 R228H allele delayed motor neuron death, as shown by quantification of Choline Acetyltransferase (ChAT)-positive motor neurons from the L4-L5 lumbar segments of the spinal cord (TBK1$^{R228H/R228H}$; SOD1^{G93A} mice have significantly more motor neurons per ventral horn compared to SOD1^{G93A} mice at P100 and P145) (Figures 2C and 2D). These results are in contrast to a previous study, where the heterozygous deletion of TBK1 in the SOD1^{G93A} background had no effect on motor neuron survival and ameliorated motor performance, although it accelerated early NMJ denervation (Brenner et al., 2019). We note that our studies are focused on point mutations that affect the kinase activity of TBK1 as opposed to hemizygous loss of TBK1 protein.

Conditional Deletion of TBK1 in Motor Neurons Is Sufficient to Accelerate Disease Onset in SOD1^{G93A} Mice

In order to understand the contribution of loss of TBK1 function in motor neurons alone to the observed phenotypes, we generated mice bearing a conditional TBK1 deletion in motor neurons (TBK1 cKO). Specifically, we bred TBK1$^{flox/flox}$ mice to ChAT-Cre mice to selectively delete the *Tbk1* gene in cholinergic neurons, which include motor neurons (Figure 3A). Immunostaining of spinal cord sections confirmed the absence of TBK1 protein in motor neurons (Figure 3B). We found that TBK1 cKO mice are viable and do not display obvious neurological or motor defects. However, when the TBK1 cKO mice were crossed with SOD1^{G93A} mice, a substantial acceleration (36.5%) in the onset of hind limb tremor in double mutant mice was observed compared to SOD1^{G93A} mice (Figure 3C; median onset was 111 days in TBK1 cWT; SOD1^{G93A} versus 70.5 days in TBK1 cKO; SOD1^{G93A} littermates). Complete loss of TBK1 from motor neurons of SOD1 mice also significantly diminished motor performance in the rotarod test, wire hang grip strength, and grip strength force assays (Figures 3D–3F). We note that complete loss of TBK1 from motor neurons alone had more impact on disease onset and motor performance of SOD1^{G93A} mice compared to the homozygous knockin of TBK1 R228H mutation in all cells. Despite early disease onset and diminished motor performance, TBK1 cKO; SOD1^{G93A} mice did not exhibit a shortened lifespan compared to SOD1^{G93A} mice (Figure 3G). However, disease duration (from disease onset to disease end stage) significantly increased in TBK1 cKO; SOD1^{G93A}mice compared to TBK1 cWT; SOD1^{G93A} mice (Figure 3H).

Conditional Deletion of TBK1 in Motor Neurons Accelerates Denervation of Neuromuscular Junctions and Motor Neuron Death

Consistent with the reduced motor performance of TBK1 cKO; SOD1^{G93A} mice compared to TBK1 cWT; SOD1^{G93A} mice, denervation of NMJs at the TA muscle occurred earlier in the

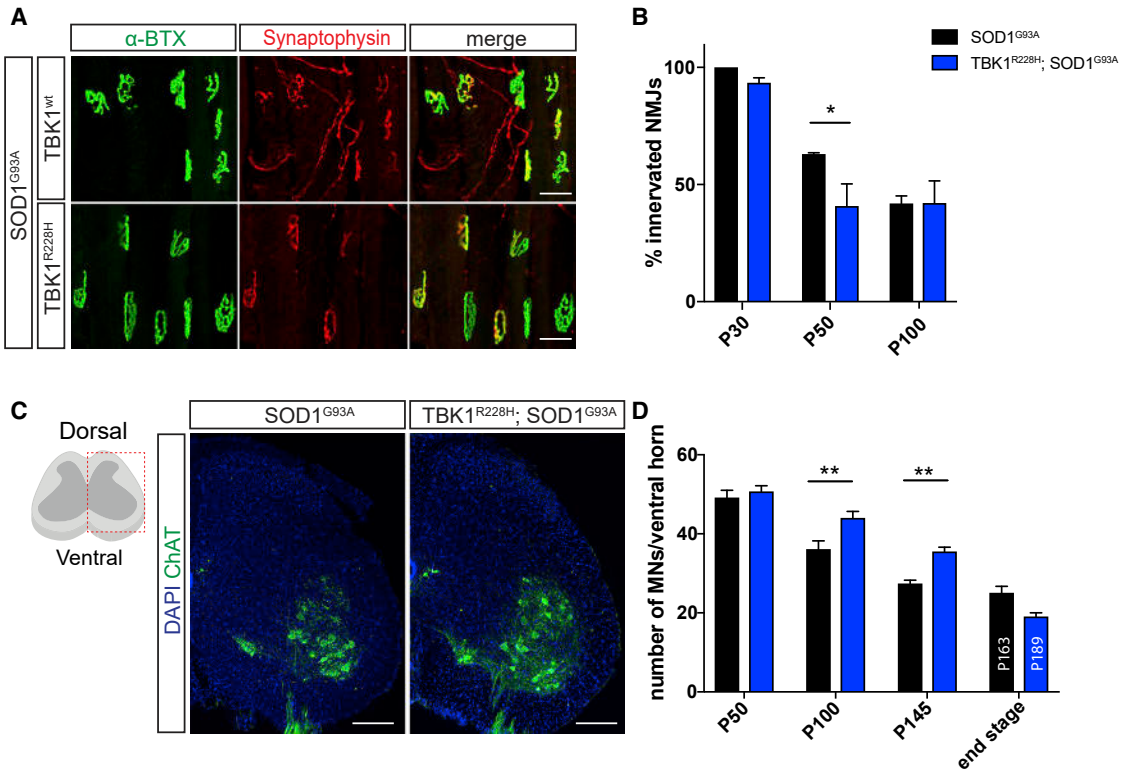

Figure 2. TBK1 R228H Mutation Accelerates Denervation of NMJs but Delays MN Death in SOD1^{G93A} Mice

(A) Tibialis anterior NMJs revealed by presynaptic synaptophysin (red) and postsynaptic α-bungarotoxin (green) labeling. Scale bars, 50 μm.

(B) Quantification of the percentage of innervated NMJs.

(C) Staining of lumbar spinal cord sections from mice of the indicated genotypes with an antibody against ChAT (green). DAPI, blue. Scale bars, 200 μm.

(D) Quantification of ventral horn motor neurons in TBK1$^{R228H/R228H}$; SOD1^{G93A} and SOD1^{G93A} mice. Data are shown as mean ± SEM (two-way ANOVA, Sidak's post hoc test). n = 3–5 animals per genotype per time point.

*p = 0.0332, **p = 0.0021, ***p = 0.0002, ****p < 0.0001.

TBK1 cKO; SOD1^{G93A} mice starting from early stages of the disease (Figures 4A and 4B; 29.1% innervated NMJs at P50 in TBK1 cKO; SOD1^{G93A} versus 64.17% in TBK1 cWT; SOD1^{G93A} mice). Increased NMJ denervation was similarly observed at P100 (Figure 4B; 16% innervated NMJs at P100 in TBK1 cKO; SOD1^{G93A} versus 36.83% in TBK1 cWT; SOD1^{G93A} mice). Histological analysis of transverse sections of TA muscles also revealed that muscle denervation is accompanied by muscle atrophy, as indicated by a significant increase in the number of fibers with smaller cross-sectional area and decreased number of larger fibers in TBK1 cKO; SOD1^{G93A} animals (Figures S3A and S3B). We conclude that deletion of TBK1 in motor neurons is sufficient to accelerate denervation of NMJs of vulnerable ALS muscles in SOD1^{G93A} mice.

Quantification of ChAT-positive motor neurons from the L4-L5 lumbar segments of the spinal cord during disease progression (P30–P145) revealed that motor neuron loss occurred earlier in TBK1 cKO; SOD1^{G93A} mice compared to TBK1 cWT; SOD1^{G93A} littermates (Figures 4D and 4E; the mean number of motor neurons/ventral horn was 40.81 versus 41.53 at P50, 22.36 versus 30.5 at P100, and 20.07 versus 26.81 at P150, respectively). These data show that, in contrast to the reduced rate of motor neuron death observed in the TBK1 knockin mice, where TBK1 activity is concomitantly lost from motor neurons and all other cell types in the spinal cord, selective loss of TBK1 function from motor neurons accelerates motor neuron death in SOD1 mice. Consistent with the absence of motor defects in TBK1 cKO mice without the SOD1 mutation, the loss of TBK1 from motor neurons of WT mice did not affect innervation of NMJs at the vulnerable TA muscle (Figure 4C), morphology of the NMJs (Figures S3C and S3D), or motor neuron survival (Figure 4F). Thus, the impact of the complete loss of TBK1 function on motor neuron viability and muscle innervation requires the presence of mutant SOD1 protein in this mouse model.

TBK1 Is Active in Ubiquitinated Inclusions Targeted for Autophagy in Motor Neurons

To understand the mechanisms that lead to accelerated disease onset and decreased motor performance of TBK1 mutant mice, we initially focused on the cell-autonomous effects of loss of TBK1 function. We previously reported that in the SOD1 mouse model, "round bodies" (RBs), composed of protein aggregates and autophagosome components, can be detected in vulnerable motor neurons at early stages of ALS disease progression using antibodies against ubiquitin, the autophagy receptors p62 and NBR1, and the autophagosomal proteins LC3 and GABARAPL1

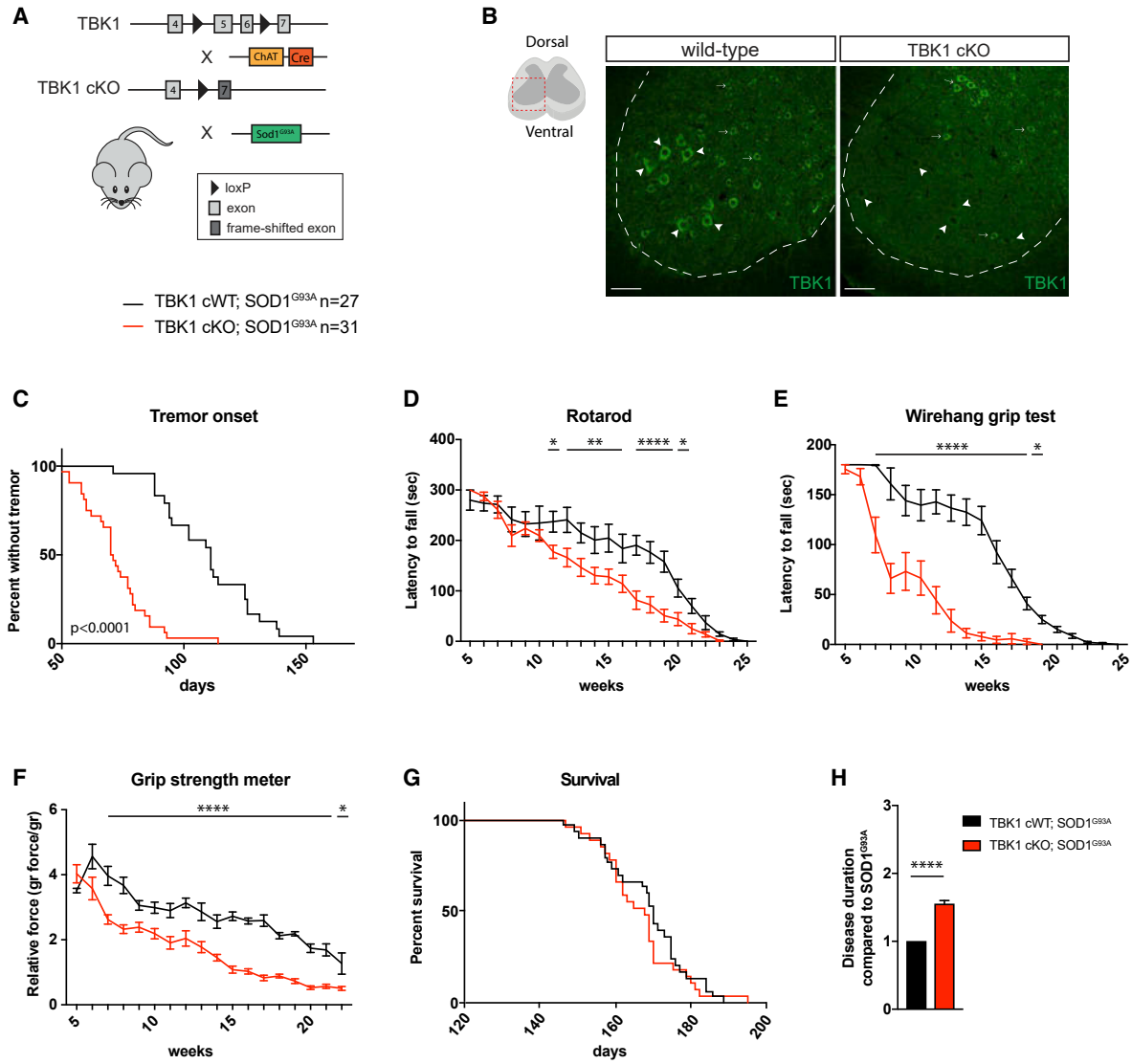

Figure 3. Deletion of TBK1 in Motor Neurons Accelerates Early Motor Defects in SOD1^{G93A} Mice but Extends Disease Duration

(A) Breeding scheme to obtain conditional deletion of TBK1 from motor neurons of SOD1 mice. Different colors indicate different genotypes.

(B) Immunofluorescent staining of the ventral horn of the lumbar spinal cord shows absence of TBK1 (green) from motor neurons of TBK1 cKO mice. Arrowheads point to large cholinergic neurons, and arrows point to smaller non-cholinergic cells. Scale bars, 50 μm.

(C) Kaplan-Meier plot showing effects of TBK1 conditional deletion on disease onset. Log-rank test = 45.86, $p < 0.0001$.

(D–F) TBK1 cKO; SOD1^{G93A} mice showed reduced performance on motor tests such as rotarod (D), wirehang grip test (E), and grip strength force assay (F). Results are shown as mean ± SEM; *p = 0.0332, **p = 0.0021, ***p = 0.0002, ****p < 0.0001; multiple t tests.

(G) Genotype had no effect on survival. Log-rank test = 0.487, p = 0.4853.

(H) Disease duration is extended by 1.5-fold in TBK1 cKO; SOD1^{G93A} mice relative to TBK1 cWT; SOD1^{G93A} controls. n = 27–31 animals per genotype, sex balanced.

(Rudnick et al., 2017). Previous *in vitro* studies have shown that autophagy receptors are phosphorylated by TBK1, and this phosphorylation enhances the clearance of autophagic cargos (reviewed in Oakes et al., 2017). Our recent study revealed that TBK1 mutations can affect the phosphorylation of autophagy receptors (Ye et al., 2019), raising the possibility that these mutations might impact selective autophagy. Immunofluorescent analysis detected discrete foci of p-TBK1 (phospho-serine 172, a marker for activated TBK1) that co-localized with the autophagy receptor p62, ubiquitin, and the autophagosomal protein LC3 in ChAT+ neurons of the lumbar spinal cord of P50 SOD1^{G93A} mice (Figures 5A and 5B). These data indicate that early in ALS disease progression, TBK1 is active in motor neurons and is directly involved in the autophagy pathway that targets protein aggregates for clearance.

TBK1 Is Required for Normal Proteostasis in Motor Neurons

Immunofluorescent staining of spinal cord sections using antibodies against pS403 p62 and pS177 OPTN (known TBK1

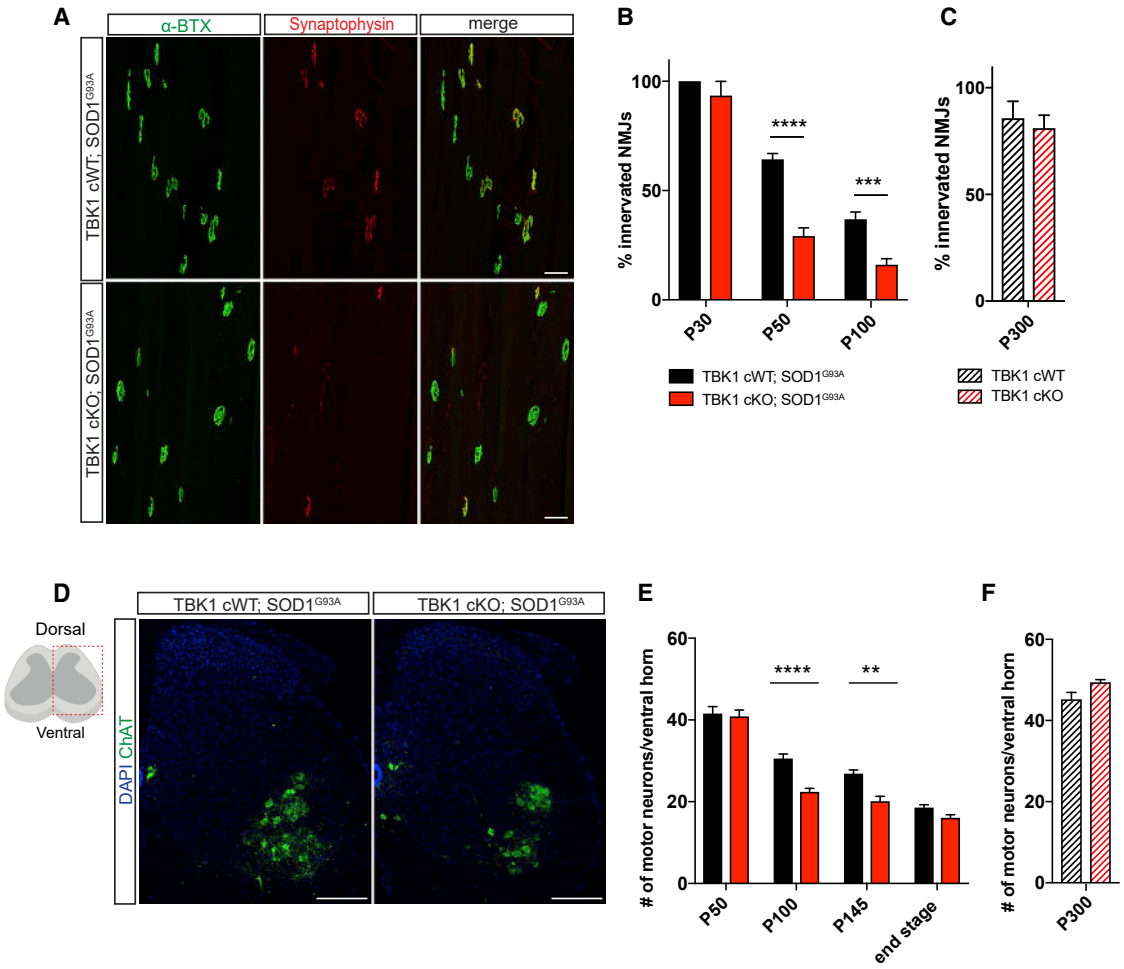

Figure 4. Functional Defects Associated with TBK1 Deletion in Motor Neurons

(A) Tibialis anterior NMJs revealed by presynaptic synaptophysin (red) and postsynaptic α-bungarotoxin (green) labeling. Scale bars, 50 μm.

(B and C) Quantification of the percentage of innervated NMJs in TBK1 cKO; SOD1^{G93A} and TBK1cWT; SOD1^{G93A} mice at the indicated time points (B) and in 10-month-old TBK1 cWT and TBK1 cKO and WT mice (C).

(D) Staining of lumbar spinal cord sections with an antibody against ChAT (green). DAPI, blue. Scale bars, 200 μm.

(E and F) Quantification of the number of motor neurons/ventral horn in TBK1 cKO; SOD1^{G93A} and TBK1 cWT; SOD1^{G93A} mice at the indicated time points (E) and in 10-month-old TBK1 cKO and WT mice (F). Data are shown as mean ± SEM (two-way ANOVA, Sidak's post hoc test). *p = 0.0332, **p = 0.0021, ***p = 0.0002, ****p < 0.0001 n = 3–5 animals per genotype per time point.

targets involved in autophagy) revealed that both autophagy receptors are phosphorylated in SOD1^{G93A} motor neurons but not in those lacking TBK1 (Figures 5C and 5D). Consistent with the observed partial loss of kinase activity of the TBK1 R228H mutant protein (Figures 1G and 1H), we also detected reduced pS403 p62 and pS177 OPTN in TBK1$^{R228H/R228H}$; SOD1^{G93A} mice (Figures 5C, 5D, and S4A), an effect specific to the loss of TBK1 but not IKKε (Figures S4A–S4C). Finally, we observed that loss of TBK1 function from motor neurons (MNs) of SOD1 mice—in either TBK1 conditional deletion animals or mutant TBK1 knockin animals—led to a substantial increase in the number of RBs (Figures 5E and 5F; the mean number of ubiquitinated aggregates per cell was 12.11 in SOD1^{G93A} versus 23.42 in TBK1 cKO; SOD1^{G93A} and 22.3 in TBK1$^{R228H/R228H}$; SOD1^{G93A} at P50). Significantly, these inclusions appear earlier in motor neurons of TBK1 cKO; SOD1^{G93A} and TBK1$^{R228H/R228H}$; SOD1^{G93A} mice compared to SOD1^{G93A} animals and persist throughout disease progression (Figure 5G; mean percentage of MNs with RBs was 6.71 in TBK1 WT versus 33.77 in TBK1 cKO and 41.16 in TBK1 R228H at P30, 40.33 in TBK1 WT versus 52.74 in TBK1 cKO and 45.49 in TBK1 R228H at P50, 7.55 in TBK1 WT versus 25.26 in TBK1 cKO and 28.61 in TBK1 R228H at P100, and 0.81 in TBK1 WT versus 10.79 in TBK1 cKO and 10.72 in TBK1 R228H at end stage). Evidence that the aggregates contain SOD1 protein was provided by filter trap analysis (Medinas et al., 2018) of spinal cord extracts from WT, SOD1^{G93A}, and TBK1$^{R228H/R228H}$; SOD1^{G93A} mice (Figures 5H and 5I).

We note that knocking out either individual autophagy receptors (p62 or OPTN) or the critical autophagy gene *Atg7* does not prevent the phosphorylation of TBK1 in MNs (Figure S4D).

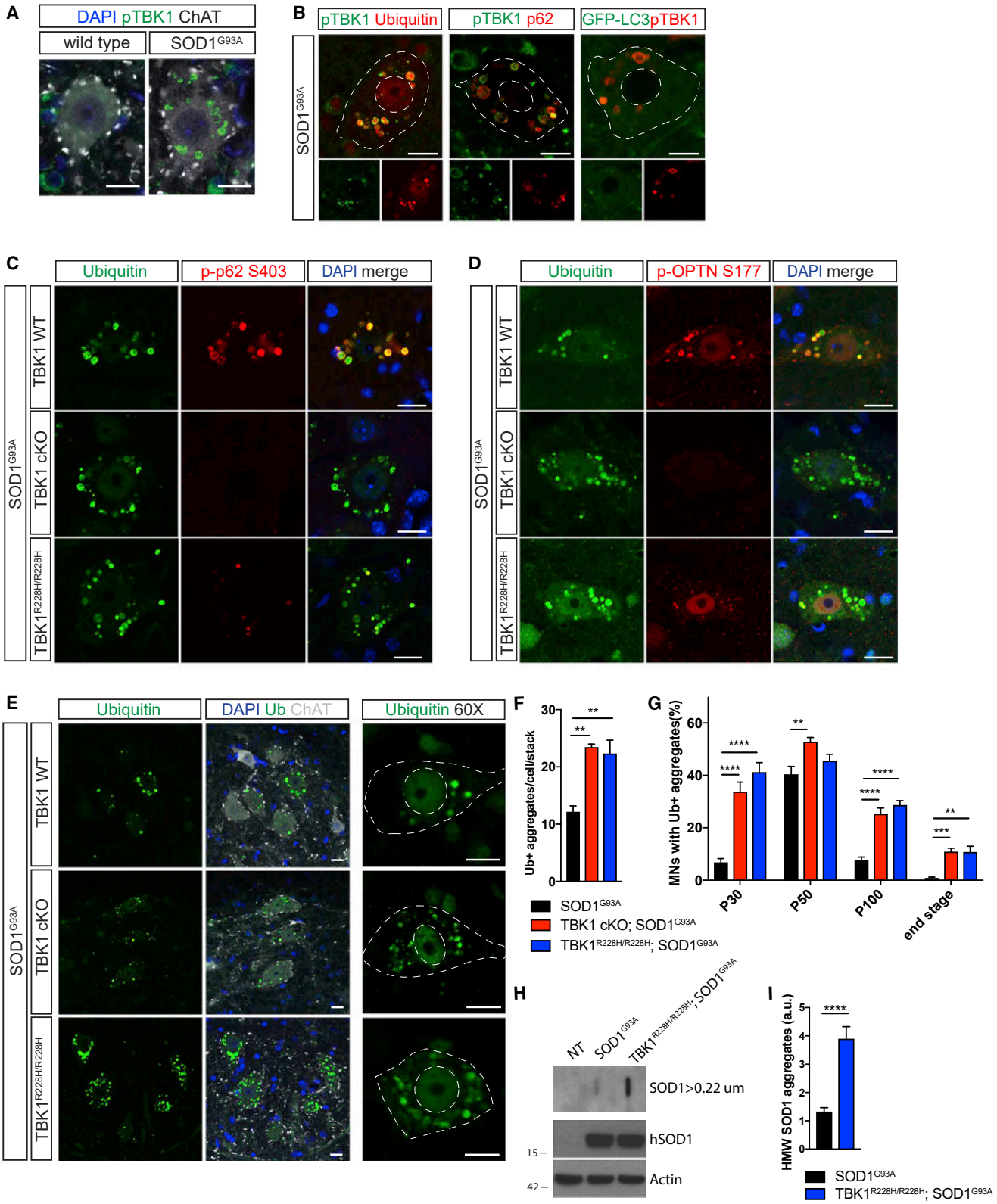

(legend on next page)

Nevertheless, TBK1 mutants led to a reduction in the phosphorylation of autophagy receptors and an increase in the accumulation of ubiquitinated aggregates in ALS motor neurons *in vivo*, likely impairing autophagic clearance.

The Absence of TBK1 in Motor Neurons Leads to an Enhanced Cellular Stress Response

RNA-seq analyses of L4-L5 spinal cords from P50 WT and mutant mice revealed an increase in transcription of a specific set of genes in the TBK1 cKO; $SOD1^{G93A}$ compared to the $SOD1^{G93A}$ spinal cord at early stages of disease (Table S1). Among these genes is ATF3, a key transcription factor involved in the cellular stress response pathway. ATF3 was previously shown to be upregulated in ALS motor neurons at the pre-symptomatic stages of neurodegeneration (Lobsiger et al., 2007). Increased levels of ATF3 mRNA were also detected early in disease in the spinal cord of $TBK1^{R228H/R228H}$; $SOD1^{G93A}$ mice (Figure 6A). Immunofluorescent staining of ATF3 in spinal cord sections revealed that it is upregulated in motor neurons containing p62 positive aggregates (Figure 6B), which also stained positive for nuclear phospho-c-Jun (p-c-Jun) (Figure 6B). We note that ATF3 and p-c-Jun signals were significantly increased in TBK1 cKO; $SOD1^{G93A}$ motor neurons as well as in $TBK1^{R228H/R228H}$; $SOD1^{G93A}$ motor neurons compared to $SOD1^{G93A}$ motor neurons at early disease stages (Figures 6C and 6D).

The cellular stress response can also induce morphological changes of organelles. For example, fragmentation of the Golgi apparatus (i.e., the transformation of the Golgi apparatus from a network of linear stacks to dispersed smaller elements) is a typical feature observed in a subset of motor neurons of ALS patients and SOD1-ALS mice, where Golgi fragmentation starts as early as 15 weeks of age (Vlug et al., 2005). To test the hypothesis that the stress response correlates with Golgi damage in motor neurons lacking TBK1, we stained spinal cord sections of 7-week-old mice for the *cis*-Golgi protein GM130 and p-c-Jun and found that the appearance of Golgi fragmentation in motor neurons significantly increased in the absence of functional TBK1, which correlates with the presence of nuclear phospho-c-Jun and the abundance of p62+ aggregates (Figures 6E–6G). These data indicate that loss of TBK1 function leads to the accelerated activation of the ATF3/p-c-Jun stress response pathway and Golgi fragmentation in $SOD1^{G93A}$ motor neurons, likely a result of increased accumulation of SOD1 aggregates due to defective autophagic clearance.

Loss of TBK1 Function in Motor Neurons Alters the Distribution of Protein Aggregates and Gliosis in the Spinal Cord at Late Disease Stages

A critical step in ALS disease progression in humans is the spread of pathology over time (Ravits, 2014). At late disease stages in the SOD1 mouse model, p62-positive, ubiquitin-positive, hSOD1-positive skein-like inclusions appear in ChAT-negative interneurons of the intermediate zone and dorsal horn of the spinal cord (Figures 7A and 7B) (Rudnick et al., 2017). Activation of microglia and astrocytes is also observed in the same spinal cord regions (Figure 7E) (Rudnick et al., 2017). We previously reported that the distribution of pathological markers (such as p62- and ubiquitin-positive inclusions and gliosis) in the spinal cord is affected by the level of autophagic activity in motor neurons (Rudnick et al., 2017). To determine whether conditional deletion of TBK1 from motor neurons or the presence of the TBK1 R228H mutation in all cell types also affect the distribution of pathology in the spinal cord, we stained the lumbar spinal cord of P150 mice for p62, the microglial marker Iba1, and the astrocyte marker GFAP. We note that the P150 time point is close to the end stage time point for both the $SOD1^{G93A}$ and TBK1 cKO; $SOD1^{G93A}$ mice but not for $TBK1^{R228H/R228H}$; $SOD1^{G93A}$ mice (end stage ~190 days; Figures 1M and 3E). A decrease in the levels of protein aggregation in interneurons and gliosis was observed in the intermediate zone and dorsal horn of P150 TBK1 cKO; $SOD1^{G93A}$ and $TBK1^{R228H/R228H}$; $SOD1^{G93A}$ compared to $SOD1^{G93A}$ mice (Figures 7C–7G). However, by P190 $TBK1^{R228H/R228H}$; $SOD1^{G93A}$ mice showed levels of protein aggregation and gliosis similar to that of $SOD1^{G93A}$ mice (Figures 7C–7G).

Dynamic changes in cell-type-specific gene expression during disease progression can also be inferred from RNA-seq data. We analyzed RNA-seq data from L4-L5 spinal cords of WT (P150), $SOD1^{G93A}$ (P150), TBK1 cKO; $SOD1^{G93A}$ (P150), and $TBK1^{R228H/R228H}$; $SOD1^{G93A}$ (P150 and P190) mice. Using spinal cord cell subtype transcriptional signatures (Rosenberg et al., 2018; Zhang et al., 2014), we observed a selective increase of astrocyte and microglial markers in $SOD1^{G93A}$ mice, which was delayed in $TBK1^{R228H/R228H}$; $SOD1^{G93A}$ mice (Figure 7H). These data suggest that the loss or reduction of TBK1 activity specifically in motor neurons is sufficient to delay the wider distribution of protein aggregates and gliosis in other regions of the spinal cord. We also found that motor neuron and other neuron markers were diminished in $SOD1^{G93A}$ mice compared to WT mice, and this depletion was significantly delayed in $TBK1^{R228H/R228H}$;

Figure 5. Autophagy Defects in $SOD1^{G93A}$ Motor Neurons Lacking WT TBK1

(A) Immunofluorescent labeling of ChAT (gray) and p-TBK1 (green) in P50 WT and $SOD1^{G93A}$ motor neurons.

(B) Co-immunostaining of p-TBK1 (red) and ubiquitin (green, first panel), p62 (green, middle panel), and LC3 (green, right panel) in $SOD1^{G93A}$ motor neurons at P50.

(C and D) Immunostaining of $SOD1^{G93A}$ motor neurons with antibodies against ubiquitin (green) and phosphorylated p62 (red, C) or phosphorylated optineurin (red, D).

(E) $SOD1^{G93A}$ spinal cord motor neurons (ChAT, gray) stained with an antibody against ubiquitin (green). The right panels show high magnification of motor neurons bearing round bodies.

(F) Quantification of round bodies/cell/stack.

(G) Quantification of motor neurons with round bodies. n = 3–5 animals per genotype.

(H) Filter trap assay (top) shows enhanced accumulation of SOD1 aggregates in the spinal cord of P50 $TBK1^{R228H/R228H}$; $SOD1^{G93A}$ compared to $SOD1^{G93A}$ mice. Western blot analysis (bottom) shows similar levels of human SOD1 and actin in the same samples.

(I) Quantification of band intensity from filter trap normalized over western blot of SOD1 in the spinal cords. n = 4 per genotype. Data are shown as mean ± SEM; *p = 0.0332, **p = 0.0021, ***p = 0.0002, ****p < 0.0001 (two-way ANOVA, Holm-Sidak's multiple comparisons test). Scale bars, 10 μm. DAPI, blue.

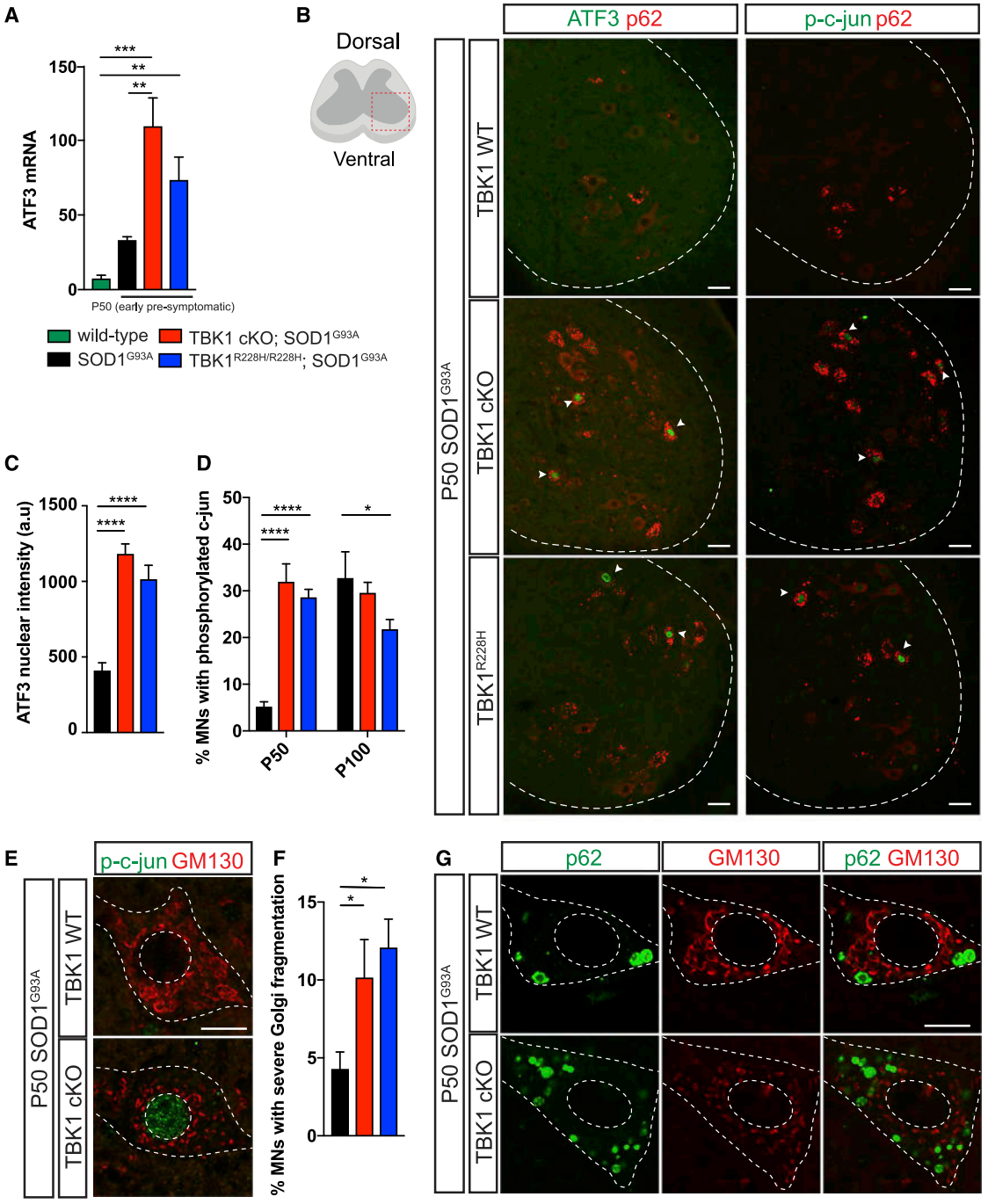

Figure 6. TBK1 Loss from Motor Neurons Accelerates the Cellular Stress Response

(A) ATF3 mRNA levels in lumbar spinal cord of WT, SOD1^{G93A}, TBK1 cKO; SOD1^{G93A}, and TBK1$^{R228H/R228H}$; SOD1^{G93A} mice.

(B) Immunofluorescent labeling of p62 (red) and ATF3 (green, left panel) or p-c-Jun (green, right panel) in lumbar spinal cord sections from the indicated genotypes at P50. Scale bars, 50 μm.

(C) Quantification of ATF3 mean nuclear intensity.

(D) Quantification of MNs with phosphorylated c-Jun.

(E) Double immunofluorescent labeling of spinal motor neurons with the Golgi marker GM130 (red) reveals severe Golgi fragmentation in motor neurons positive for p-c-Jun (green).

(F) Quantification of MNs with severe Golgi fragmentation.

(G) Double immunofluorescent labeling of spinal motor neurons with the Golgi marker GM130 (red) and p62 (green). Scale bars, 10 μm. Data are shown as mean ± SEM; *p = 0.0332, **p = 0.0021, ***p = 0.0002, ****p < 0.0001 (one-way ANOVA, Holm-Sidak's multiple comparison test).

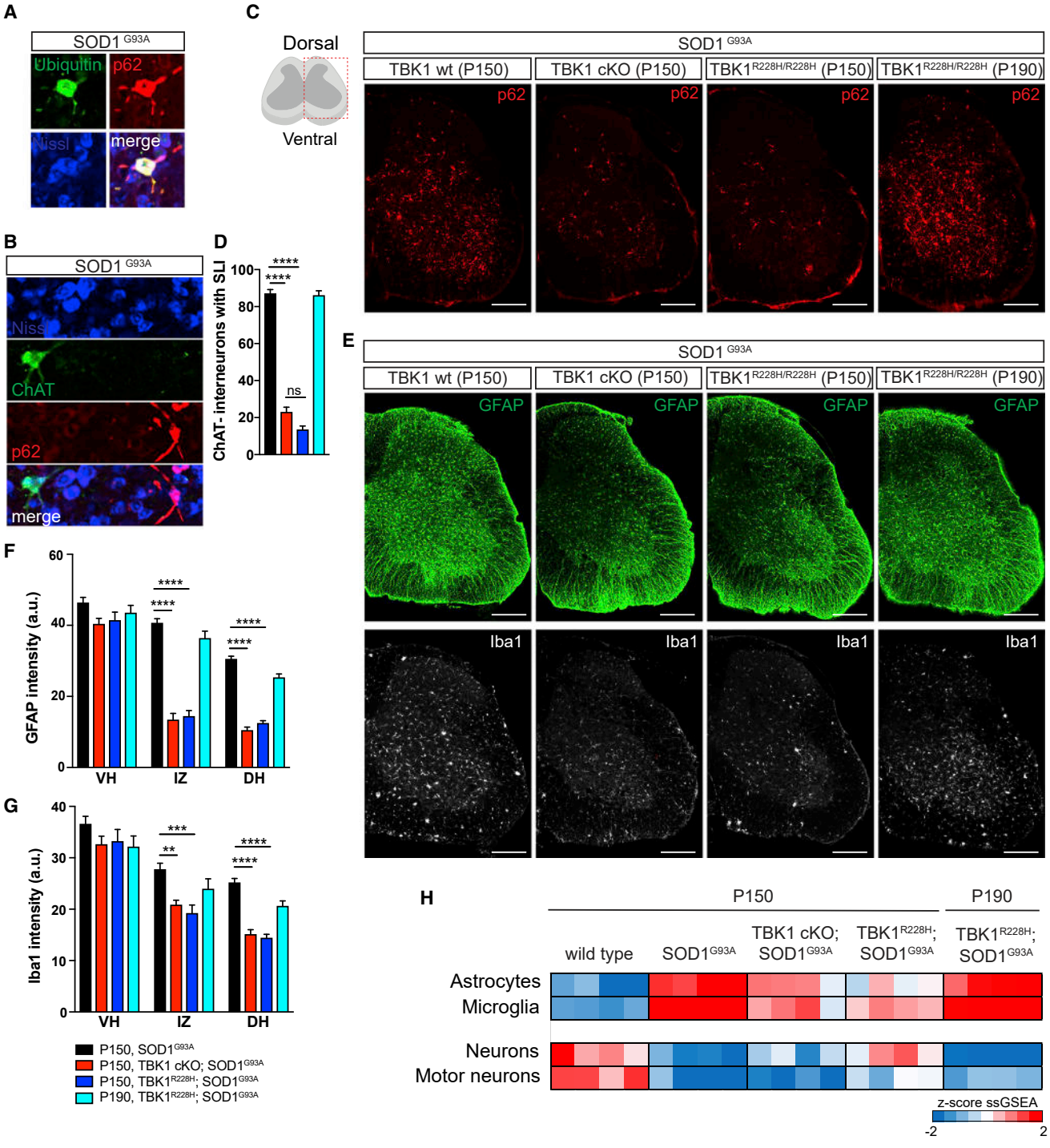

Figure 7. Cell-Autonomous Loss of TBK1 Affects Glial and Interneuron Pathology

(A) Immunofluorescent labeling of a Skein-like inclusion (SLI) with antibodies against ubiquitin (green) and p62 (red) in interneuron (blue) of the dorsal region of the spinal cord.

(B) Immunofluorescent labeling of ChAT-positive and ChAT-negative interneurons shows accumulation of SLIs (red) in non-cholinergic interneurons.

(C) Immunofluorescent labeling of lumbar spinal cord sections from the indicated genotypes with an antibody against p62 (red). Scale bars, 200 μm.

(D) Quantification of Nissl+, ChAT− interneurons with p62+ inclusions in intermediate zone (IZ) and dorsal horn (DH) of the spinal cord.

(E) Immunofluorescent labeling of GFAP (green) and Iba1 (gray) in lumbar spinal cord sections from the indicated genotypes. Scale bars, 200 μm.

(legend continued on next page)

SOD1^{G93A} mice, consistent with the delayed motor neuron death described above (Figures 7H, 4C, and 4D). These observations are consistent with reduced neuroinflammation observed in the spinal cord of TBK1$^{+/-}$; SOD1^{G93A} compared to SOD1^{G93A} mice (Brenner et al., 2019). However, our data demonstrates that the reduction of gliosis observed by Brenner et al. in the spinal cord is a non-cell-autonomous result of selective loss of TBK1 function in motor neurons.

Loss of TBK1 Function Reduces the Interferon Response in the Spinal Cord of SOD1^{G93A} Mice

Gene ontology analysis by DAVID on genes differentially downregulated in end stage TBK1$^{R228H/R228H}$; SOD1^{G93A} spinal cord, compared to the SOD1^{G93A} spinal cord, revealed that the "innate immunity," "defense response to virus," and "interferon (IFN) response" categories were the most highly enriched gene ontology (GO) terms (Figure 8A). Comparison of these genes to IFN-regulated genes (Liu et al., 2012) showed that selected genes in this pathway are upregulated in SOD1^{G93A} mice bearing the WT TBK1 gene (Table S2). Interestingly, some of these genes were recently shown to be upregulated in reactive astrocytes or microglia in aging, brain injury, or neurodegenerative diseases (Deczkowska et al., 2017; Hammond et al., 2019; Liddelow et al., 2017; Mathys et al., 2017) and in spatial transcriptomic studies of spinal cord of SOD1-ALS mice (Maniatis et al., 2019). However, we note that the induction of a subgroup of the IFN-inducible genes is markedly reduced in TBK1$^{R228H/R228H}$; SOD1^{G93A} mice (Figure 8B).

In order to gain further mechanistic insights, our bulk RNA-seq results were validated by single cell immunofluorescence and single molecule FISH (smFISH) analysis of selected targets. Specifically, we found that high levels of the transcription factor interferon activated protein 204 (IFI204) were detected in nuclei of microglia from SOD1^{G93A} mice but not in WT mice nor in TBK1$^{R228H/R228H}$; SOD1^{G93A} mice (Figures 8C and 8D). SmFISH (RNA scope) combined with immunofluorescence revealed that IRF7 and USP18 mRNAs were upregulated in microglia of SOD1^{G93A} mice compared to WT controls (Figures 8E–8H). However, this induction was significantly reduced in the absence of normal levels of functional TBK1 (Figures 8E–8H). By contrast, the expression of Lgals3, an NF-kB regulated gene known to be upregulated in microglia during neurodegeneration (Krasemann et al., 2017), is not affected by the TBK1 R228H mutation (Figures 8I and 8J). SmFISH for the transcription factor IRF7 and USP18 RNAs, combined with immunofluorescent staining of astrocytes (GFAP) or neurons (Nissl stain), revealed that USP18 levels were also reduced in astrocytes by the loss of function of TBK1 (Figures S5D and S5E). These data indicate that the TBK1 R228H loss-of-function mutation decreases the expression of selected interferon-inducible genes in microglia and to a smaller extent in astrocytes.

Western blots of protein lysates from lumbar spinal cords of end stage mice revealed that the transcription factor IRF3—which is required for type-I IFN gene expression (Au et al., 1995)—is phosphorylated in the spinal cord of SOD1^{G93A} mice. Although both TBK1 and IKKε are able to phosphorylate IRF3, the partial loss of function of TBK1—but not IKKε—is sufficient to reduce the phosphorylation of IRF3 and expression of a subset of interferon-regulated genes in the spinal cord of SOD1-ALS mice (Figure 8M).

We conclude that the interferon signaling pathway is activated in microglia and astrocytes in the spinal cord of SOD1^{G93A} mice, and the loss of TBK1 function selectively reduces the induction of a subset of interferon-inducible genes in these cells during disease progression.

DISCUSSION

Neurodegenerative disease progression is a complex process involving many different cell types in the brain and spinal cord, and dynamic changes in cell-cell interactions over time. Key intracellular pathways or drug targets at one stage of progression can be completely different at another stage. Thus, targeting a specific pathway could be beneficial at one stage and detrimental at another. We provide an interesting example of this here. We find that the loss of function of TBK1 accelerates disease progression at early times and slows progression at late times of disease in the SOD1^{G93A} ALS mouse model. An additional complication is that different cell types (for example, motor neurons and glia) respond differently to TBK1 loss-of-function mutations.

Loss of TBK1 Function in Motor Neurons Disrupts Proteostasis and Accelerates Early Stages of ALS Disease Symptoms

Our studies of disease progression in SOD1^{G93A} mice in which *Tbk1* (this study) or *Atg7* (Rudnick et al., 2017) are conditionally deleted in motor neurons provide strong support that motor neuron autophagy is a key pathway in early disease progression. The role of TBK1 in selective autophagy has been studied in both neuronal and non-neuronal cells in culture (reviewed in Oakes et al., 2017). Here we find that defects in proteostasis downstream of TBK1 in motor neurons correlate with earlier onset of cellular and pathological hallmarks of ALS. Specifically, we found that early in ALS disease progression partial loss of TBK1 kinase activity leads to hypophosphorylation of the autophagy receptors p62 and optineurin in motor neurons, which, in turn, leads to increased accumulation of protein aggregates, presumably due to the negative impact on autophagy. This increase is accompanied by the activation of the ATF3/c-*jun* stress response pathway and Golgi damage earlier in disease progression compared to the SOD1^{G93A} mouse lacking TBK1 mutations.

The transcription factor ATF3 plays an important role in mediating the cellular response to injury and stress (Hunt et al., 2012). It is unclear whether ATF3 induction in motor neurons drives pro-survival or cell death mechanisms. For example, overexpression of ATF3 in SOD1 mice resulted in delayed neuromuscular

(F and G) Quantification of GFAP (F) and Iba1 (G) intensity in the ventral horn (VH), intermediate zone (IZ), and dorsal horn (DH) of the spinal cord in arbitrary units (au). n = 3 animals per genotype, sex matched. Data are shown as mean ± SEM; ***p < 0.001, ****p < 0.0001 (two-way ANOVA, Tukey's post hoc test).

(H) Single-sample gene set enrichment analysis (ssGSEA) for cell-type-specific transcriptional signatures. Sub columns represent biological replicates.

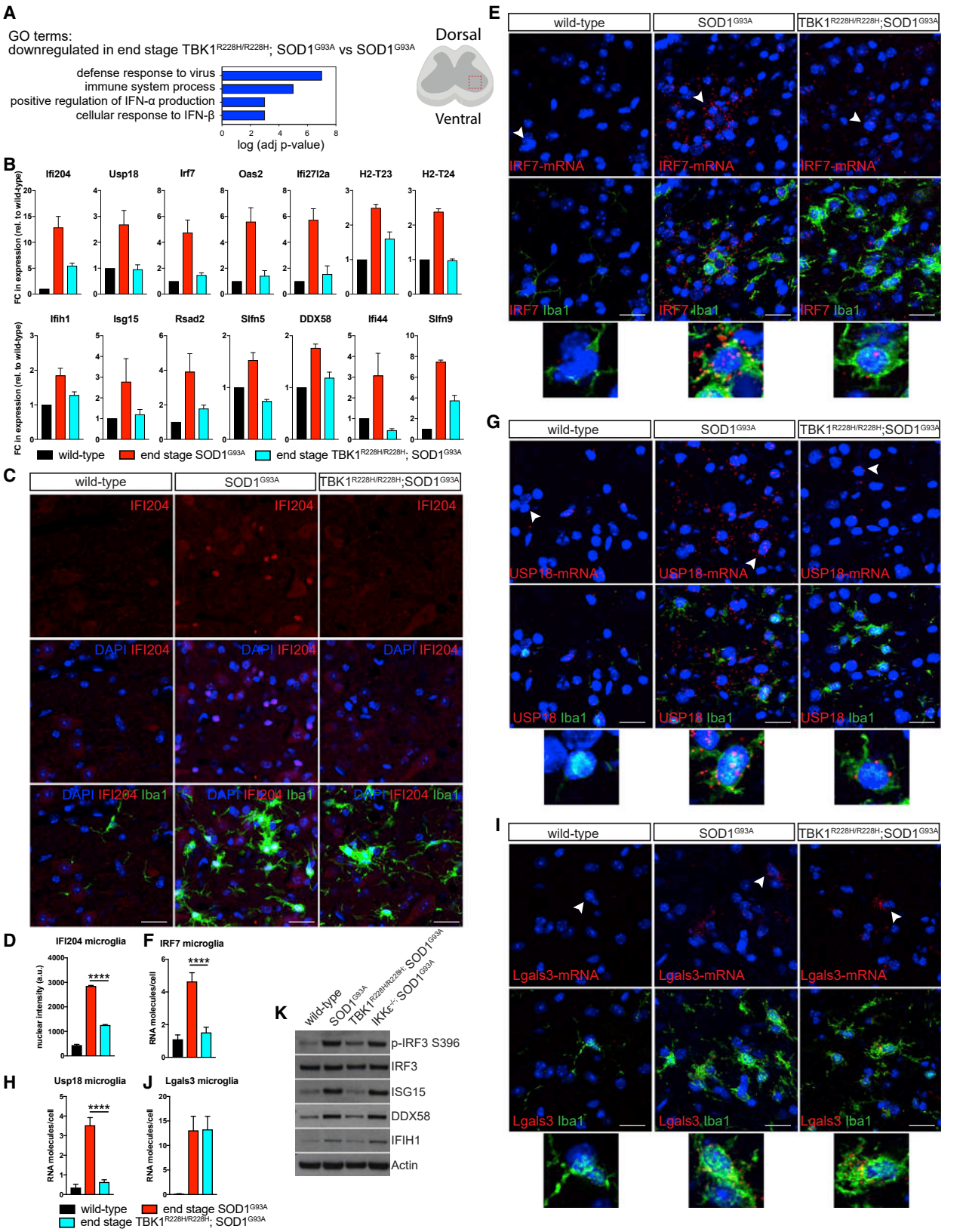

(legend on next page)

junction denervation by inducing axonal sprouting and enhancing motor neuron viability (Seijffers et al., 2014). However, in other studies of SOD1 mice ATF3 upregulation was associated with Golgi damage (van Dis et al., 2014; Mourelatos et al., 1996; Vlug et al., 2005) or with ER stress, specifically in vulnerable—but not resistant—ALS motor neurons (Saxena et al., 2009).

Golgi pathology is a prominent feature of neurodegenerative diseases, including Alzheimer's and Parkinson's disease, where Golgi fragmentation is often detected as an early event and believed to contribute to disease pathogenesis (Haase and Rabouille, 2015; Sundaramoorthy et al., 2015). Golgi damage was previously observed in motor neurons of rodent models of ALS, as well as in sporadic ALS patients and familial ALS patients bearing mutations in SOD1, FUS, or OPTN (Sundaramoorthy et al., 2015). In addition, previous studies demonstrated a correlation between the presence of TDP-43 aggregates and Golgi fragmentation in spinal motor neurons of ALS patients and in transgenic rats overexpressing human TDP-43 (Fujita et al., 2008; Tong et al., 2012). Here we show that the accumulation of SOD1 protein aggregates, activation of the cell stress response, and Golgi damage in motor neurons of SOD1^{G93A} mice are all accelerated by the selective loss of TBK1 in motor neurons.

Loss of TBK1 Function from Motor Neurons Delays Disease Propagation in the Spinal Cord

In contrast to the negative effects early in disease progression, the absence of TBK1 in motor neurons is beneficial late in this SOD1 mouse model. Our data suggests that this is a consequence, at least in part, of the impact on cell-non-autonomous effects in the spinal cord. Previous studies have led to the proposal that in ALS, pathology initiates focally and then spreads spatiotemporally (Ravits, 2014). Such disease spread has also been reported for Alzheimer's disease, Parkinson disease, tauopathies, and Huntington disease as a result of the accumulation and spread of misfolded or aggregated proteins and the accompanying neuroinflammation from a focal site to neighboring cells (Brundin et al., 2010; Polymenidou and Cleveland, 2011). Studies of *in vivo* and *in vitro* models of ALS disease have provided evidence that misfolded SOD1 aggregates propagate between cells (Ayers et al., 2014, 2016; Bidhendi et al., 2016; Grad et al., 2014; Silverman et al., 2016; Thomas et al., 2017). Our previous studies on macroautophagy showed that deletion of the essential autophagy gene *Atg7* from motor neurons leads to a decrease in the appearance of pathological protein aggregates in other cells over time in the spinal cord (Rudnick et al., 2017). Here we show that the conditional deletion of TBK1 from motor neurons similarly slows the appearance of disease hallmarks throughout the spinal cord. This could be a result of a direct effect of autophagy on formation and release of extracellular vesicles bearing protein aggregates (such as exosomes) or alternatively an indirect consequence of a reduction in the ability of stressed motor neurons with severe Golgi damage to form and release vesicles, which would lead to diminished spread of these aggregates. We note that the conditional deletion of either Atg7 or TBK1 leads to a similar increase in disease duration (1.8-fold and 1.5-fold, respectively) compared to mice with normal motor neuron autophagy. This suggests that suppression of disease spread through inhibition of motor neuron autophagy might contribute to the observed increase in disease duration. We note that conditional deletion of Atg7 in motor neurons leads to an extended lifespan in SOD1 animals, while deleting TBK1 in motor neurons does not affect survival. We speculate that this difference may result from the earlier disease onset in TBK1 cKO; SOD1^{G93A} mice compared to Atg7 cKO; SOD1^{G93A} animals (disease onset was accelerated by 36.5% in TBK1 cKO; SOD1^{G93A} and by 22% in Atg7 cKO; SOD1^{G93A} compared to SOD1^{G93A} littermates). This is likely a reflection of the pleiotropic functions of TBK1 compared to Atg7, which exclusively functions in autophagy.

Loss of TBK1 Function Reduces the Expression of Interferon-Regulated Genes

The type I interferon pathway is a major component of the cellular immune response to tissue-damaging agents, the presence of cytoplasmic DNA (Blank and Prinz, 2017), or DNA released from damaged mitochondria (West and Shadel, 2017). Chronically elevated type-I IFN response has been shown to contribute to the pathology of human CNS diseases and in animal models of neurodegeneration (Blank and Prinz, 2017; Owens et al., 2014). In addition, persistent expression or excessive levels of IFN in the CNS has been linked to pathological changes, including aging (Baruch et al., 2014; Deczkowska et al., 2017), neurodegeneration, and microgliosis (Akwa et al., 1998). Moreover, chronic challenge of SOD1 mice with LPS—a potent inducer of the IFN response—exacerbated disease progression and motor axon degeneration (Nguyen et al., 2004), while deletion of the IFN receptor gene extended the lifespan of SOD1 mice (Wang et al., 2011). Treatment of human ALS patients with IFN-α or -β caused severe inflammation and accelerated disease progression (Beghi et al., 2000; Poutiainen et al., 1994). Thus, abnormal activation of the IFN pathway in ALS and other neurodegenerative diseases appears to play a major role in disease progression.

Here we show that loss of TBK1 kinase activity in all cells of the spinal cord reduces the phosphorylation of the transcription factor IRF3. TBK1$^{R228H/R228H}$; SOD1^{G93A} mice display a diminished

Figure 8. TBK1 R228H Mutation Decreases the Induction of IFN-Regulated Genes in the Spinal Cord Microglia of SOD1 Mice

(A) GO analysis of genes significantly downregulated at disease end stage in TBK1$^{R228H/R228H}$; SOD1^{G93A} mice compared to SOD1^{G93A} mice.

(B) Bar plot of fold changes (compared to WT) of selected IFN-regulated genes in TBK1$^{R228H/R228H}$; SOD1^{G93A} (P190, end stage) and SOD1^{G93A} (P150, end stage) lumbar spinal cord.

(C and D) Immunostaining (C) and relative quantification (D) of mean nuclear intensity signal for IFI204 (red) in microglia (green) in the indicated genotypes at the end stage of the disease.

(E–L) Single molecule FISH (RNAscope) using RNA probes for IRF7 (E), USP18 (F), and Lgals3 (I) (red) combined with immunostaining of microglia (green) and relative quantification (F, H, J) of number of RNA molecules per cell. Scale bars, 10 μm. Panels below are higher magnification of cells indicated by white arrowheads. Data are shown as mean ± SEM; ***$p < 0.001$, ****$p < 0.0001$ (one-way ANOVA, Holm-Sidak's multiple comparison test).

(M) Western blot showing diminished phosphorylation of IRF3 and expression of selected proteins encoded by ISGs in end stage TBK1$^{R228H/R228H}$; SOD1^{G93A} compared to SOD1^{G93A} and IKK$\varepsilon^{-/-}$; SOD1^{G93A} mice.

induction of a subset of interferon stimulated genes (ISGs) in microglia and astrocytes compared to $SOD1^{G93A}$ mice. In addition, a slower rate of motor neuron loss, prolonged disease duration (2.7-fold), and extended lifespan are observed in $TBK1^{R228H/R228H}$; $SOD1^{G93A}$ mice.

Taken together, our data support the hypothesis that the decrease in the interferon response in spinal cord microglia and astrocytes of $TBK1^{R228H/R228H}$; $SOD1^{G93A}$ mice is a result of the decrease in the mutant TBK1 activity, and this leads to the slowing of neurodegeneration, contributing to the extension of survival of SOD1 mice late in disease progression.

At the present time, DNA sequence variants in more than 25 different genes have been linked to ALS. These genes function in many distinct cellular pathways yet lead to a common spectrum of disease phenotypes. Therefore, the identification of disease mechanisms on which multiple ALS genes converge, is the key for the discovery of potential therapeutic targets. In this study we showed that early in ALS disease progression the loss of TBK1 disrupts autophagy in motor neurons and accelerates ALS pathology. However, as the severity of the disease advances with age, the loss of TBK1 function is beneficial due to a diminished immune response. We therefore provide an example of how multiple pathways can be targeted through manipulation of a single gene, and how modulating specific pathways in ALS can be beneficial or detrimental depending on the stage of disease progression.

STAR★METHODS

Detailed methods are provided in the online version of this paper and include the following:

- KEY RESOURCES TABLE
- LEAD CONTACT AND MATERIAL AVAILABILITY
- EXPERIMENTAL MODEL AND SUBJECT DETAILS
  - Animals
  - Cell lines
- METHOD DETAILS
  - Generation of TBK1 knock-in mice
  - Behavioral Assessment
  - Immunohistochemistry
  - Motor neuron Analyses
  - Neuromuscular Junction Analyses
  - Quantification of Astrogliosis and Microgliosis
  - Transfection and Luciferase assay
  - *In vitro* kinase assays
  - Filter Trap Assay
  - Analysis of Protein Levels
  - Gene-Expression Analysis
  - Single molecule FISH combined with immunofluorescence
- QUANTIFICATION AND STATISTICAL ANALYSIS
- DATA AND CODE AVAILABILITY

SUPPLEMENTAL INFORMATION

Supplemental Information can be found online at https://doi.org/10.1016/j.neuron.2020.03.005.

ACKNOWLEDGMENTS

We thank Drs. Isaac Chiu, Stavros Lomvardas, David Hirsh, and Joseph Puccini for their critical reading of the manuscript. We would also like to thank Dr. Ai Yamamoto for helpful discussion and Dr. Frank Baas for providing patient fibroblasts. We thank Emily Birnbaum and Chris Griffey for technical help. This work was supported by grants from Project ALS (PRALS 2017-09) and Takeda Pharmaceuticals (1000344702). V.G. is a recipient of a Milton Safenowitz postdoctoral fellowship from ALSA, and D.C. is a recipient of an NIH Path to Independence Award K99/R00 K99GM121815. The generation and development of the CRISPR/Cas9 mutant mouse models was supported by the Jackson Laboratory Precision Genetics Center Grant U54OD020351-04. We acknowledge the support of Aamir Zuberi (Jackson Laboratory) and of The Jackson Laboratory Genome Engineering Technology group. Jackson Lab Core facility costs were defrayed by Cancer Center Support Grant CA034196.

AUTHOR CONTRIBUTIONS

V.G. and T.M. designed the project; V.G, E.K., J.Y., D.C., and N.D.R. performed experiments; V.G. and E.K. analyzed data; V.G., D.C., S.O.K., and P.G. analyzed sequencing data; C.M.L. generated mutant mice; V.G. and T.M. wrote the manuscript; and J.Y. and N.D.R provided critical comments.

DECLARATION OF INTERESTS

The authors declare no competing interests.

Received: July 11, 2019
Revised: December 30, 2019
Accepted: March 9, 2020
Published: March 27, 2020

REFERENCES

Akwa, Y., Hassett, D.E., Eloranta, M.L., Sandberg, K., Masliah, E., Powell, H., Whitton, J.L., Bloom, F.E., and Campbell, I.L. (1998). Transgenic expression of IFN-alpha in the central nervous system of mice protects against lethal neurotropic viral infection but induces inflammation and neurodegeneration. J. Immunol. *161*, 5016–5026.

Au, W.C., Moore, P.A., Lowther, W., Juang, Y.T., and Pitha, P.M. (1995). Identification of a member of the interferon regulatory factor family that binds to the interferon-stimulated response element and activates expression of interferon-induced genes. Proc. Natl. Acad. Sci. USA *92*, 11657–11661.

Ayers, J.I., Fromholt, S., Koch, M., DeBosier, A., McMahon, B., Xu, G., and Borchelt, D.R. (2014). Experimental transmissibility of mutant SOD1 motor neuron disease. Acta Neuropathol. *128*, 791–803.

Ayers, J.I., Fromholt, S.E., O'Neal, V.M., Diamond, J.H., and Borchelt, D.R. (2016). Prion-like propagation of mutant SOD1 misfolding and motor neuron disease spread along neuroanatomical pathways. Acta Neuropathol. *131*, 103–114.

Baruch, K., Deczkowska, A., David, E., Castellano, J.M., Miller, O., Kertser, A., Berkutzki, T., Barnett-Itzhaki, Z., Bezalel, D., Wyss-Coray, T., et al. (2014). Aging. Aging-induced type I interferon response at the choroid plexus negatively affects brain function. Science *346*, 89–93.

Beghi, E., Chiò, A., Inghilleri, M., Mazzini, L., Micheli, A., Mora, G., Poloni, M., Riva, R., Serlenga, L., Testa, D., and Tonali, P.; Italian Amyotrophic Lateral Sclerosis Study Group (2000). A randomized controlled trial of recombinant interferon beta-1a in ALS. Neurology *54*, 469–474.

Bidhendi, E.E., Bergh, J., Zetterström, P., Andersen, P.M., Marklund, S.L., and Brännström, T. (2016). Two superoxide dismutase prion strains transmit amyotrophic lateral sclerosis-like disease. J. Clin. Invest. *126*, 2249–2253.

Blank, T., and Prinz, M. (2017). Type I interferon pathway in CNS homeostasis and neurological disorders. Glia *65*, 1397–1406.

Blokhuis, A.M., Groen, E.J.N., Koppers, M., van den Berg, L.H., and Pasterkamp, R.J. (2013). Protein aggregation in amyotrophic lateral sclerosis. Acta Neuropathol. *125*, 777–794.

Boillée, S., Yamanaka, K., Lobsiger, C.S., Copeland, N.G., Jenkins, N.A., Kassiotis, G., Kollias, G., and Cleveland, D.W. (2006). Onset and progression in inherited ALS determined by motor neurons and microglia. Science *312*, 1389–1392.

Bonnard, M., Mirtsos, C., Suzuki, S., Graham, K., Huang, J., Ng, M., Itié, A., Wakeham, A., Shahinian, A., Henzel, W.J., et al. (2000). Deficiency of T2K leads to apoptotic liver degeneration and impaired NF-kappaB-dependent gene transcription. EMBO J. *19*, 4976–4985.

Brenner, D., Sieverding, K., Bruno, C., Lüningschrör, P., Buck, E., Mungwa, S., Fischer, L., Brockmann, S.J., Ulmer, J., Bliederhäuser, C., et al. (2019). Heterozygous *Tbk1* loss has opposing effects in early and late stages of ALS in mice. J. Exp. Med. *216*, 267–278.

Brundin, P., Melki, R., and Kopito, R. (2010). Prion-like transmission of protein aggregates in neurodegenerative diseases. Nat. Rev. Mol. Cell Biol. *11*, 301–307.

Cirulli, E.T., Lasseigne, B.N., Petrovski, S., Sapp, P.C., Dion, P.A., Leblond, C.S., Couthouis, J., Lu, Y.F., Wang, Q., Krueger, B.J., et al.; FALS Sequencing Consortium (2015). Exome sequencing in amyotrophic lateral sclerosis identifies risk genes and pathways. Science *347*, 1436–1441.

Clement, A.M., Nguyen, M.D., Roberts, E.A., Garcia, M.L., Boillée, S., Rule, M., McMahon, A.P., Doucette, W., Siwek, D., Ferrante, R.J., et al. (2003). Wild-type nonneuronal cells extend survival of SOD1 mutant motor neurons in ALS mice. Science *302*, 113–117.

de Majo, M., Topp, S.D., Smith, B.N., Nishimura, A.L., Chen, H.J., Gkazi, A.S., Miller, J., Wong, C.H., Vance, C., Baas, F., et al. (2018). ALS-associated missense and nonsense TBK1 mutations can both cause loss of kinase function. Neurobiology of Aging *71*, 266.e1–266.e10.

Deczkowska, A., Matcovitch-Natan, O., Tsitsou-Kampeli, A., Ben-Hamo, S., Dvir-Szternfeld, R., Spinrad, A., Singer, O., David, E., Winter, D.R., Smith, L.K., et al. (2017). Mef2C restrains microglial inflammatory response and is lost in brain ageing in an IFN-I-dependent manner. Nat. Commun. *8*, 717.

Fitzgerald, K.A., McWhirter, S.M., Faia, K.L., Rowe, D.C., Latz, E., Golenbock, D.T., Coyle, A.J., Liao, S.M., and Maniatis, T. (2003). IKKepsilon and TBK1 are essential components of the IRF3 signaling pathway. Nat. Immunol. *4*, 491–496.

Freischmidt, A., Wieland, T., Richter, B., Ruf, W., Schaeffer, V., Müller, K., Marroquin, N., Nordin, F., Hübers, A., Weydt, P., et al. (2015). Haploinsufficiency of TBK1 causes familial ALS and fronto-temporal dementia. Nat. Neurosci. *18*, 631–636.

Fujita, Y., Mizuno, Y., Takatama, M., and Okamoto, K. (2008). Anterior horn cells with abnormal TDP-43 immunoreactivities show fragmentation of the Golgi apparatus in ALS. J. Neurol. Sci. *269*, 30–34.

Geloso, M.C., Corvino, V., Marchese, E., Serrano, A., Michetti, F., and D'Ambrosi, N. (2017). The dual role of microglia in ALS: Mechanisms and therapeutic approaches. Front. Aging Neurosci. *9*, 242.

Grad, L.I., Yerbury, J.J., Turner, B.J., Guest, W.C., Pokrishevsky, E., O'Neill, M.A., Yanai, A., Silverman, J.M., Zeineddine, R., Corcoran, L., et al. (2014). Intercellular propagated misfolding of wild-type Cu/Zn superoxide dismutase occurs via exosome-dependent and -independent mechanisms. Proc. Natl. Acad. Sci. USA *111*, 3620–3625.

Haase, G., and Rabouille, C. (2015). Golgi fragmentation in ALS motor neurons. New mechanisms targeting microtubules, tethers, and transport vesicles. Front. Neurosci. *9*, 448.

Hammond, T.R., Dufort, C., Dissing-Olesen, L., Giera, S., Young, A., Wysoker, A., Walker, A.J., Gergits, F., Segel, M., Nemesh, J., et al. (2019). Single-Cell RNA Sequencing of Microglia throughout the Mouse Lifespan and in the Injured Brain Reveals Complex Cell-State Changes. Immunity *50*, 253–271.

Heiman-Patterson, T.D., Sher, R.B., Blankenhorn, E.A., Alexander, G., Deitch, J.S., Kunst, C.B., Maragakis, N., and Cox, G. (2011). Effect of genetic background on phenotype variability in transgenic mouse models of amyotrophic lateral sclerosis: a window of opportunity in the search for genetic modifiers. Amyotroph. Lateral Scler. *12*, 79–86.

Heo, J.-M., Ordureau, A., Paulo, J.A., Rinehart, J., and Harper, J.W. (2015). The PINK1-PARKIN Mitochondrial Ubiquitylation Pathway Drives a Program of OPTN/NDP52 Recruitment and TBK1 Activation to Promote Mitophagy. Mol. Cell *60*, 7–20.

Hunt, D., Raivich, G., and Anderson, P.N. (2012). Activating transcription factor 3 and the nervous system. Front. Mol. Neurosci. *5*, 7.

Krasemann, S., Madore, C., Cialic, R., Baufeld, C., Calcagno, N., El Fatimy, R., Beckers, L., O'Loughlin, E., Xu, Y., Fanek, Z., et al. (2017). The TREM2-APOE Pathway Drives the Transcriptional Phenotype of Dysfunctional Microglia in Neurodegenerative Diseases. Immunity *47*, 566–581.

Lazarou, M., Sliter, D.A., Kane, L.A., Sarraf, S.A., Wang, C., Burman, J.L., Sideris, D.P., Fogel, A.I., and Youle, R.J. (2015). The ubiquitin kinase PINK1 recruits autophagy receptors to induce mitophagy. Nature *524*, 309–314.

Liddelow, S.A., Guttenplan, K.A., Clarke, L.E., Bennett, F.C., Bohlen, C.J., Schirmer, L., Bennett, M.L., Münch, A.E., Chung, W.-S., Peterson, T.C., et al. (2017). Neurotoxic reactive astrocytes are induced by activated microglia. Nature *541*, 481–487.

Liu, S.Y., Sanchez, D.J., Aliyari, R., Lu, S., and Cheng, G. (2012). Systematic identification of type I and type II interferon-induced antiviral factors. Proc. Natl. Acad. Sci. USA *109*, 4239–4244.

Lobsiger, C.S., Boillée, S., and Cleveland, D.W. (2007). Toxicity from different SOD1 mutants dysregulates the complement system and the neuronal regenerative response in ALS motor neurons. Proc. Natl. Acad. Sci. USA *104*, 7319–7326.

Maniatis, S., Äijö, T., Vickovic, S., Braine, C., Kang, K., Mollbrink, A., Fagegaltier, D., Andrusivová, Ž., Saarenpää, S., Saiz-Castro, G., et al. (2019). Spatiotemporal dynamics of molecular pathology in amyotrophic lateral sclerosis. Science *364*, 89–93.

Mathys, H., Adaikkan, C., Gao, F., Young, J.Z., Manet, E., Hemberg, M., De Jager, P.L., Ransohoff, R.M., Regev, A., and Tsai, L.-H. (2017). Temporal Tracking of Microglia Activation in Neurodegeneration at Single-Cell Resolution. Cell Rep. *21*, 366–380.

Matsumoto, G., Shimogori, T., Hattori, N., and Nukina, N. (2015). TBK1 controls autophagosomal engulfment of polyubiquitinated mitochondria through p62/SQSTM1 phosphorylation. Hum. Mol. Genet. *24*, 4429–4442.

McWhirter, S.M., Fitzgerald, K.A., Rosains, J., Rowe, D.C., Golenbock, D.T., and Maniatis, T. (2004). IFN-regulatory factor 3-dependent gene expression is defective in Tbk1-deficient mouse embryonic fibroblasts. Proc. Natl. Acad. Sci. USA *101*, 233–238.

Medinas, D.B., Rozas, P., Martínez Traub, F., Woehlbier, U., Brown, R.H., Bosco, D.A., and Hetz, C. (2018). Endoplasmic reticulum stress leads to accumulation of wild-type SOD1 aggregates associated with sporadic amyotrophic lateral sclerosis. Proc. Natl. Acad. Sci. USA *115*, 8209–8214.

Moore, A.S., and Holzbaur, E.L.F. (2016). Dynamic recruitment and activation of ALS-associated TBK1 with its target optineurin are required for efficient mitophagy. Proc. Natl. Acad. Sci. USA *113*, E3349–E3358.

Mourelatos, Z., Gonatas, N.K., Stieber, A., Gurney, M.E., and Dal Canto, M.C. (1996). The Golgi apparatus of spinal cord motor neurons in transgenic mice expressing mutant Cu,Zn superoxide dismutase becomes fragmented in early, preclinical stages of the disease. Proc. Natl. Acad. Sci. USA *93*, 5472–5477.

Nguyen, M.D., D'Aigle, T., Gowing, G., Julien, J.P., and Rivest, S. (2004). Exacerbation of motor neuron disease by chronic stimulation of innate immunity in a mouse model of amyotrophic lateral sclerosis. J. Neurosci. *24*, 1340–1349.

Oakes, J.A., Davies, M.C., and Collins, M.O. (2017). TBK1: a new player in ALS linking autophagy and neuroinflammation. Mol. Brain *10*, 5.

Owens, T., Khorooshi, R., Wlodarczyk, A., and Asgari, N. (2014). Interferons in the central nervous system: a few instruments play many tunes. Glia *62*, 339–355.

Polymenidou, M., and Cleveland, D.W. (2011). The seeds of neurodegeneration: prion-like spreading in ALS. Cell *147*, 498–508.

Poutiainen, E., Hokkanen, L., Niemi, M.-L., and Färkkilä, M. (1994). Reversible cognitive decline during high-dose α-interferon treatment. Pharmacol. Biochem. Behav. *47*, 901–905.

Ravits, J. (2014). Focality, stochasticity and neuroanatomic propagation in ALS pathogenesis. Exp. Neurol. *262B*, 121–126.

Richter, B., Sliter, D.A., Herhaus, L., Stolz, A., Wang, C., Beli, P., Zaffagnini, G., Wild, P., Martens, S., Wagner, S.A., et al. (2016). Phosphorylation of OPTN by TBK1 enhances its binding to Ub chains and promotes selective autophagy of damaged mitochondria. Proc. Natl. Acad. Sci. USA *113*, 4039–4044.

Rosenberg, A.B., Roco, C.M., Muscat, R.A., Kuchina, A., Sample, P., Yao, Z., Graybuck, L.T., Peeler, D.J., Mukherjee, S., Chen, W., et al. (2018). Single-cell profiling of the developing mouse brain and spinal cord with split-pool barcoding. Science *360*, 176–182.

Rudnick, N.D., Griffey, C.J., Guarnieri, P., Gerbino, V., Wang, X., Piersaint, J.A., Tapia, J.C., Rich, M.M., and Maniatis, T. (2017). Distinct roles for motor neuron autophagy early and late in the $SOD1^{G93A}$ mouse model of ALS. Proc. Natl. Acad. Sci. USA *114*, E8294–E8303.

Saxena, S., Cabuy, E., and Caroni, P. (2009). A role for motoneuron subtype-selective ER stress in disease manifestations of FALS mice. Nat. Neurosci. *12*, 627–636.

Schindelin, J., Arganda-Carreras, I., Frise, E., Kaynig, V., Longair, M., Pietzsch, T., Preibisch, S., Rueden, C., Saalfeld, S., Schmid, B., et al. (2012). Fiji: an open-source platform for biological-image analysis. Nat. Methods *9*, 676–682.

Seijffers, R., Zhang, J., Matthews, J.C., Chen, A., Tamrazian, E., Babaniyi, O., Selig, M., Hynynen, M., Woolf, C.J., and Brown, R.H., Jr. (2014). ATF3 expression improves motor function in the ALS mouse model by promoting motor neuron survival and retaining muscle innervation. Proc. Natl. Acad. Sci. USA *111*, 1622–1627.

Sharma, S., tenOever, B.R., Grandvaux, N., Zhou, G.P., Lin, R., and Hiscott, J. (2003). Triggering the interferon antiviral response through an IKK-related pathway. Science *300*, 1148–1151.

Silverman, J.M., Fernando, S.M., Grad, L.I., Hill, A.F., Turner, B.J., Yerbury, J.J., and Cashman, N.R. (2016). Disease Mechanisms in ALS: Misfolded SOD1 Transferred Through Exosome-Dependent and Exosome-Independent Pathways. Cell. Mol. Neurobiol. *36*, 377–381.

Solis, M., Romieu-Mourez, R., Goubau, D., Grandvaux, N., Mesplede, T., Julkunen, I., Nardin, A., Salcedo, M., and Hiscott, J. (2007). Involvement of TBK1 and IKKepsilon in lipopolysaccharide-induced activation of the interferon response in primary human macrophages. Eur. J. Immunol. *37*, 528–539.

Sundaramoorthy, V., Sultana, J.M., and Atkin, J.D. (2015). Golgi fragmentation in amyotrophic lateral sclerosis, an overview of possible triggers and consequences. Front. Neurosci. *9*, 400.

Taylor, J.P., Brown, R.H., Jr., and Cleveland, D.W. (2016). Decoding ALS: from genes to mechanism. Nature *539*, 197–206.

Tenoever, B.R., Ng, S.-L., Chua, M.A., McWhirter, S.M., García-Sastre, A., and Maniatis, T. (2007). Multiple functions of the IKK-related kinase IKKepsilon in interferon-mediated antiviral immunity. Science *315*, 1274–1278.

Thomas, E.V., Fenton, W.A., McGrath, J., and Horwich, A.L. (2017). Transfer of pathogenic and nonpathogenic cytosolic proteins between spinal cord motor neurons in vivo in chimeric mice. Proc. Natl. Acad. Sci. USA *114*, E3139–E3148.

Tong, J., Huang, C., Bi, F., Wu, Q., Huang, B., and Zhou, H. (2012). XBP1 depletion precedes ubiquitin aggregation and Golgi fragmentation in TDP-43 transgenic rats. J. Neurochem. *123*, 406–416.

Valdez, G., Tapia, J.C., Kang, H., Clemenson, G.D., Jr., Gage, F.H., Lichtman, J.W., and Sanes, J.R. (2010). Attenuation of age-related changes in mouse neuromuscular synapses by caloric restriction and exercise. Proc. Natl. Acad. Sci. USA *107*, 14863–14868.

van Dis, V., Kuijpers, M., Haasdijk, E.D., Teuling, E., Oakes, S.A., Hoogenraad, C.C., and Jaarsma, D. (2014). Golgi fragmentation precedes neuromuscular denervation and is associated with endosome abnormalities in SOD1-ALS mouse motor neurons. Acta Neuropathol. Commun. *2*, 38.

Vlug, A.S., Teuling, E., Haasdijk, E.D., French, P., Hoogenraad, C.C., and Jaarsma, D. (2005). ATF3 expression precedes death of spinal motoneurons in amyotrophic lateral sclerosis-SOD1 transgenic mice and correlates with c-Jun phosphorylation, CHOP expression, somato-dendritic ubiquitination and Golgi fragmentation. Eur. J. Neurosci. *22*, 1881–1894.

Wang, R., Yang, B., and Zhang, D. (2011). Activation of interferon signaling pathways in spinal cord astrocytes from an ALS mouse model. Glia *59*, 946–958.

West, A.P., and Shadel, G.S. (2017). Mitochondrial DNA in innate immune responses and inflammatory pathology. Nat. Rev. Immunol. *17*, 363–375.

Wild, P., Farhan, H., McEwan, D.G., Wagner, S., Rogov, V.V., Brady, N.R., Richter, B., Korac, J., Waidmann, O., Choudhary, C., et al. (2011). Phosphorylation of the autophagy receptor optineurin restricts Salmonella growth. Science *333*, 228–233.

Xu, D., Jin, T., Zhu, H., Chen, H., Ofengeim, D., Zou, C., Mifflin, L., Pan, L., Amin, P., Li, W., et al. (2018). TBK1 Suppresses RIPK1-Driven Apoptosis and Inflammation during Development and in Aging. Cell *174*, 1477–1491.e19.

Yamanaka, K., Chun, S.J., Boillee, S., Fujimori-Tonou, N., Yamashita, H., Gutmann, D.H., Takahashi, R., Misawa, H., and Cleveland, D.W. (2008). Astrocytes as determinants of disease progression in inherited amyotrophic lateral sclerosis. Nat. Neurosci. *11*, 251–253.

Ye, J., Cheung, J., Gerbino, V., Ahlsén, G., Zimanyi, C., Hirsh, D., and Maniatis, T. (2019). Effects of ALS-associated TANK binding kinase 1 mutations on protein-protein interactions and kinase activity. Proc. Natl. Acad. Sci. USA *116*, 24517–24526.

Zhang, Y., Chen, K., Sloan, S.A., Bennett, M.L., Scholze, A.R., O'Keeffe, S., Phatnani, H.P., Guarnieri, P., Caneda, C., Ruderisch, N., et al. (2014). An RNA-sequencing transcriptome and splicing database of glia, neurons, and vascular cells of the cerebral cortex. J. Neurosci. *34*, 11929–11947.

STAR★METHODS

KEY RESOURCES TABLE

REAGENT or RESOURCE	SOURCE	IDENTIFIER
Antibodies		
TBK1	Abcam	Cat# ab40676; RRID: AB_776632
p-TBK1 S172	Cell Signaling	Cat# 5483; RRID: AB_10693472
GFAP	Abcam	Cat# ab4674; RRID: AB_304558
ChAT	Millipore	Cat# AB144P; RRID: AB_2079751
Optineurin	Abcam	Cat# ab23666; RRID: AB_447598
p-IRF3 S396	Cell Signaling	Cat# 4947; RRID: AB_823547
p-IRF3 S386	Abcam	Cat# ab76493; RRID: AB_1523836
p-p62 S403 (clone4F6)	Millipore	Cat# MABC186-I
p-p62 S403	Cell Signaling	Cat# 39786; RRID: AB_2799162
p-Optineurin S177	Cell Signaling	Cat# 57548; RRID: AB_2799529
Iba1	Abcam	Cat# ab5076; RRID: AB_2224402
Iba1	Wako	Cat# 019-19741; RRID: AB_839504
Synaptophysin	SY Synaptic Systems	Cat# 101004; RRID: AB_1210382
α-bungarotoxin conjugated to Alexa fluor 488	Thermo Fisher	Cat# B13422
p-c-Jun S63	Cell Signaling	Cat# 9261; RRID: AB_2130162
p62	Abcam	Cat# ab56416; RRID: AB_945626
ATF3	Abcam	Cat# ab207434; RRID: AB_2734728
Ubiquitin FK2	Enzo Life Sciences	Cat# BML-PW8810; RRID: AB_10541840
GM-130	BD	Cat# 610823; RRID: AB_398142
Critical Commercial Assays		
SMARTer Stranded Total RNA-Seq Pico input mammalian RNA kit	Takara-Bio	Cat# 634411
RNAScope Multiplex Fluorescent V2 Assay	ACD	Cat# 323100
Deposited Data		
Sequencing data	This paper	GEO: GSE146141
Experimental Models: Cell Lines		
Primary Fibroblasts	Dr. Frank Baas	N/A
HEK293T cells	ATCC	Cat# CRL-1573; RRID: CVCL_0045
Experimental Models: Organisms/Strains		
Mouse: C57BL/6J-Tbk1 em3Lutzy /1J	This paper	Cat# Jax 027080; RRID: IMSR_JAX:027080
Mouse: C57BL/6J-Tbk1 em6Lutzy /J	This paper	Cat# Jax 027983; RRID: IMSR_JAX:027983
Mouse: B6.Cg-Tg(SOD1*G93A)1Gur/J	Jackson Labs	Cat# Jax 004435; RRID: IMSR_JAX:004435
Mouse: B6;129S6-Chattm2(cre)Lowl/J	Jackson Labs	Cat# Jax 006410; RRID: IMSR_JAX:006410
Mouse: C57BL/6-Tbk1tm1.1 mr	Taconic	Cat# 11131; RRID: IMSR_TAC:11131
Mouse: B6.Cg-Ikbketm1Tman/J	Maniatis lab	Cat# Jax 006908; RRID: IMSR_JAX:006908
Oligonucleotides		
CRISPR $gRNA_{G217R}$ TCTAAACGGCAGCGACCCCG (antisense strand)	This paper	N/A
CRISPR donor DNA_{G217R} accatcagaagaagtacggggctaccgttgat ctgtggagtgttggagtgacattctaccatgcag ccacg**A**ggtcgctgccgtttagacccttcgagg ggcctcggaggaacaaagaagtaat	This paper	N/A

(*Continued on next page*)

Continued

REAGENT or RESOURCE	SOURCE	IDENTIFIER
CRISPR gRNA$_{R228H}$ GTTCCTCCGAGGCCCCTCGA (antisense strand)	This paper	N/A
CRISPR donor DNA$_{R228H}$ gttggagtgacattctaccatgcagccacggggtc gctgccgtttagacccttcgaggggcctc**AT**agg aacaaagaagtaatgtaagcacctctgcgtctgc cgttagacggggtttctgatg	This paper	N/A
Software and Algorithms		
CANJI	Rudnick et al., 2017	N/A
GraphPad Prism	GraphPad Software	https://www.graphpad.com/scientific-software/prism/; RRID: SCR_002798
FIJI	Schindelin et al., 2012	http://fiji.sc; RRID: SCR_002285

LEAD CONTACT AND MATERIAL AVAILABILITY

Further information and requests for resources and reagents should be directed to and will be fulfilled by the Lead Contact, Tom Maniatis (tm2472@columbia.edu). The TBK1 knock-in G217R and R228H mouse lines generated in this study have been deposited to Jackson Labs (C57BL/6J-Tbk1em3Lutzy/1J, stock number 027080, and C57BL/6J-Tbk1em6Lutzy/J, stock number 027983).

EXPERIMENTAL MODEL AND SUBJECT DETAILS

Animals

All mouse experimental procedures were performed in accordance to the Columbia University Medical Center, Columbia Zuckerman Institute and The Jackson Laboratory Institutional Animal Care and Use Committees. Newly generated TBK1 knock-in mutant mouse strains are available from the Jackson Laboratory (Bar Harbor, ME) stock 027080 (C57BL/6J-Tbk1 em3Lutzy /1J) and 027983 (C57BL/6J-Tbk1 em6Lutzy /J) and the isogenic control mouse strain C57BL/6J (Stock 000664). Mice transgenic for human SOD1G93A (B6.Cg-Tg(SOD1*G93A)1Gur/J, stock number 00435) and ChAT-Cre mice (B6;129S6-Chattm2(cre)Lowl/J; stock number 006410) were acquired from Jackson Laboratory (Bar Harbor, ME). TBK1 flox mice (C57BL/6-Tbk1tm1.1 mr; stock number 11131) were obtained from Taconic (NY). IKK$\varepsilon^{-/-}$ mice were previously generated in our lab (Tenoever et al., 2007) and deposited at Jackson Laboratory (B6.Cg-Ikbketm1Tman/J, stock number 006908), p62$^{-/-}$ mice were a gift of Jaekyoon Shin of Sungkyunkwan University School of Medicine and Samsung Biomedical Research Institute, Suwon, Korea. OPTN$^{-/-}$ mice were a gift of Neil Shneider (Columbia University). TNFR$^{-/-}$ mice were a gift of Ellen Niederberger (Klinikum der Goethe-Universität Frankfurt, Germany) and Jonathan Budzik (UC Berkley). ChAT-Cre and TBK1 flox mice were backcrossed five generations to obtain C57BL/6 congenic mouse lines prior to analysis. TBK1 flox mice were bred to ChAT-Cre mice to generate mice deficient for TBK1 in the motor neurons. These mice were then bred to SOD1^{G93A} mice to generate SOD1 transgenic mice deficient for TBK1 in the motor neurons. Male and female mice were used for all experiments and experimental groups were sex balanced. Animals were provided with food and water *ad libitum*. Body weight was recorded twice a week throughout disease progression. During late-stage disease, diet was supplemented with gel-based food. Disease end-stage was determined by loss of righting reflex for more than 15 s or when 30% of body weight was lost, whichever was reached soonest.

Cell lines

HEK293T cells and primary fibroblasts derived from G217R TBK1 mutation carriers (males) (a gift from Dr. Frank Baas of Leiden University Medical Center in the Netherlands) were cultured in Dulbecco's Modified Eagle Medium (DMEM) containing 10% Fetal Bovine Serum.

METHOD DETAILS

Generation of TBK1 knock-in mice

CRISPR/Cas9 endonuclease mediated genome editing of the murine Tbk1 gene was performed using sequence specific guide RNAs with the appropriate donor oligonucleotides and plasmids expressing Cas9 microinjected into the cytoplasm of C57BL/6J-derived single cell zygotes containing well recognized pronuclei and transferred to pseudopregnant females. Correctly targeted founder mice were identified by PCR amplification of the target region following by DNA sequencing and further bred to C57BL/6J for 2 generations.

Behavioral Assessment

Tremor was assessed qualitatively by allowing mice to rest their forelimbs on the cage top and observing hind limbs. Motor balance, strength and coordination of TBK1 cKO; SOD1^{G93A} mice were assessed using an accelerating Rotarod apparatus (Ugo Basile 7560) set at a speed of 4 rpm with acceleration up to 40 rpm over 300 s. For TBK1 knock-in mice an accelerating Rotarod apparatus (Harvard Apparatus 760770) with the same settings was used. Longest latency was recorded, 300 s being the maximum. At 4 weeks, mice were trained for 3 days, two attempts each. After training, mice were subjected to Rotarod three times a day once a week from 5 weeks to 24 weeks. Muscular strength was tested by the hanging-wire test. Each mouse was placed on a wire grid and gently inverted. The grid was suspended 30 cm above soft bedding and the latency to fall was timed. Each mouse was given 3 attempts for a maximum of 180 s. After one training session at 4 weeks, the animals were assessed once a week from 5 weeks to when they could not grip. Forelimb grip strength was measured using a digital grip strength meter (Columbus Instruments, 0167-005L) which measures the maximum force applied by the mouse on the grid. The highest value obtained in three consecutive trials was normalized against mouse body weight. Mice were tested once a week from 5 weeks of age to end stage. Rotarod, hanging wire test and grip strength were each assessed on different days of the week.

Immunohistochemistry

Mice were perfused transcardially with first phosphate-buffered saline (PBS), then 4% paraformaldehyde (PFA) in PBS after being deeply anesthetized using tribromoethanol (300mg/kg). Spinal cord was dissected and post-fixed overnight at 4°C in 4% PFA. Using ventral root anatomy, the L4-L5 lumbar region was isolated and embedded in 4% agarose (WorldWide Medical Products, Bristol, PA). Free-floating 70 μm transverse sections were collected using a vibratome (Leica VT 1200 S). Tissue sections were incubated in blocking solution (100 mM Tris-HCl pH 7.5, 150 mM NaCl, 0.5% Triton X-100, 5% Donkey serum). For spinal cord samples, combinations of the following primary antibodies were used: ChAT (Millipore AB144P, 1:250), GFAP (Abcam ab4674, 1:500), Iba1 (Wako Chemicals, 1:500), p62 (Abcam ab91526 and ab56416, 1:500), ubiquitin FK2 (Enzo Life Sciences, 1:500), p-c-Jun Ser63 (Cell Signaling 9261, 1:100), p-TBK1/NAK ser172 (Cell Signaling D52C2, 1:50), Synaptophysin (Synaptic Systems 101004, 1:500), TBK1 (abcam 1:100), ATF3 (Abcam ab207434, 1:200), GM130 (BD, 1:300), p-P62 S403 (Millipore MABC186-I, 1:200), p-OPTN S177 (Cell Signaling 57548, 1:100). Primary antibody incubations were performed for two consecutive overnights at room temperature. After washing, secondary antibody incubation overnight at room temperature. Secondary antibodies used were raised in donkey and conjugated to Alexa Fluor 405, 488, 568, 633 or 647 (Thermo Fisher). Neurotrace 435/455 blue fluorescent Nissl stain (Thermo Fisher, 1:500) was included with secondary antibodies for pan-neuronal staining for some experiments. Sections were mounted on slides with Fluoromount-G (Southern Biotech, Birmingham, Alabama) prior to imaging.

Tibialis Anterior and Soleus muscles were dissected and washed overnight in PBS prior to successive incubations in 15% and 30% sucrose in PBS for cryopreservation. Then muscles were embedded in OCT compound (Sakura, Torrance, CA) and frozen at −80°C. A freezing microtome was used to collect 30 μm section onto Superfrost Plus Micro Slides (VWR, Radnor, PA). Primary antibody incubations were performed overnight at 4°C and after washing, secondary antibody incubation for 2 h at room temperature. α-bungarotoxin conjugated to Alexa fluor 488 (Thermo Fisher, 1:500) was included during secondary antibody incubation for visualization of motor end plates in muscles.

Motor neuron Analyses

Manual analysis of images of spinal cord section imaged by confocal microscopy using 20X objective. Neurons positive for ChAT in the lateral motor column were traced individually in the plane at which the nucleolus was most visible. For analysis of intracellular aggregates, circular p62 structures were considered to be RBs. Linear p62 structures present in proximal dendrites were considered to be SLIs. Analysis of p62 aggregates was subsequently verified by manual inspection of each neuron at 60 × magnification. Quantification of RBs was performed by researchers blinded to genotype, and the number of ubiquitin+, p62+ inclusions in motor neurons was counted in the plane at which the nucleolus was most visible.

Neuromuscular Junction Analyses

Muscle sections stained with synaptophysin and α-bungarotoxin were imaged with an Olympus FV1000 confocal microscope using a 10x objective, and individual images were stitched together to reconstruct the entire muscle using FluoView software. The resulting images were processed using CANJI, a custom image analysis suite developed using ImageJ, R, and Shiny (Rudnick et al., 2017). NMJs were considered to be innervated if at least 10% of the α-bungarotoxin–labeled motor endplate was overlapped by synaptophysin-labeled presynaptic terminal. To analyze NMJ morphology, muscle sections were imaged using a 40x objective and maximum intensity projections of confocal stacks were created using ImageJ. NMJs were considered moderately fragmented if composed of 2-4 AChR clusters or severely fragmented if composed of 5 or more AChR islands and/or a segment of the postsynapse showing severe abnormalities such as small and/or irregularly shaped AChR clusters (Valdez et al., 2010).

Quantification of Astrogliosis and Microgliosis

Spinal cord sections stained with antibodies against GFAP and Iba1 were imaged by confocal microscopy using a 20x objective, and pixel intensities were maintained within a linear range to ensure accurate quantification. Individual images were stitched together to reconstruct the entire section, and regions of interest corresponding to the ventral horn, intermediate zone, and dorsal horn were

superimposed onto maximum-intensity projections. Subsequently, mean fluorescence intensity for each region was determined using Fiji (Schindelin et al., 2012).

Transfection and Luciferase assay

Transfection experiments were carried out with Lipofectamine 3000 transfection reagent (Invitrogen) according to manufacturer's manual. For reporter assays, 293T cells (seeded in 96-well plates, 45,000 cells/well) were transfected with TBK1 expression constructs together with IFN-β promoter and HSV TK promoter-driven Renilla luciferase constructs. Luciferase activity was measured 24 h after transfection with Dual-Glo luciferase assay system (Promega) by a BioTek synergy HT plate reader.

In vitro kinase assays

Kinase assays were conducted in a buffer system of 20 mM HEPES, pH 7.5, 20 mM β-Glycerophosphate, 0.1 mM Na_3VO_4, 10mM $MgCl_2$ and 50 μM ATP, with recombinant TBK1 and IRF3, OPTN or GST-p62 as substrates at 30°C for increasing time. The reaction was terminated by adding equal amount of 2XSDS loading buffer. Phosphorylation of target proteins was analyzed by western blot probed with phospho-specific antibodies.

Filter Trap Assay

Filter Trap Assay of SOD1 aggregates was performed as described in (Medinas et al., 2018) with some modifications. Briefly, mouse spinal cord was dissected out and stored frozen at −80°C until analysis. The tissue was homogenized in 400 μL of TEN buffer (10 mM Tris-HCl, 1 mM EDTA, 10 mM NaCl, pH 8.0, containing protease and phosphatase inhibitors) by mechanical disruption using a glass douncer on ice. After homogenization, the tissue extract was diluted to different fractions: 1) 1:1 dilution of 150 μL homogenate into TEN buffer containing the non-ionic detergent Nonidet P-40 (NP-40) and iodoacetamide (0.5% and 50 mM final concentrations, respectively) for analysis of disulfide-dependent HMW protein aggregates, and 2) 1:1 dilution of 150 μL homogenate in TEN buffer containing NP-40 (also to a final concentration of 0.5%) for analysis of total protein. The fractions were sonicated at minimum power for 15 s on ice. Fraction 1 was incubated for 20 min at Room temperature, in the dark. Fraction 2 was incubated for 20 min at 4°C. Both fractions were centrifuged at 2,000 rcf at 4°C. Protein concentration of the supernatant was determined by the Pierce BCA Protein Assay kit (ThermoFisher, 23225). For Filter Trap 50 μg of proteins were diluted in PBS 1%SDS to a final volume of 200 μL and filtered through 0.22 μm acetate cellulose membrane under vacuum using a dot-blot apparatus. For western blot, 10 μg of proteins were prepared in Sample Buffer.

Analysis of Protein Levels

Proteins were resolved by SDS/PAGE using 4%–12% Bis-Tris gels and were transferred to PVDF membranes (Bio-Rad) using an X-cell II Blot module transfer unit (Thermo Fisher). Membranes were incubated with the following primary antibodies: TBK1, p-TBK1 S172, IRF3, p-IRF3 S368, actin-HRP, optineurin, p62. Bands were visualized using HRP-conjugated secondary antibodies (GE Healthcare Life Sciences) and quantified using ImageJ.

Gene-Expression Analysis

Lumbar spinal cords were dissected from each mouse genotype in quadruplicate. RNA was isolated using TRIzol (Thermo Fisher). RNA concentration and integrity were assessed on RNA 6000 Chips using an Agilent 2100 Bioanalyzer (Agilent Technologies). Sequencing libraries for total RNA were made using the SMARTer Stranded Total RNA-Seq Pico input mammalian RNA kit. The quality of all the libraries was assessed by bioanalyzer and quantified using a combination of bioanalyzer and qubit. Multiplexed libraries were sequenced on a NEXT-Seq 500/550.

Illumina real-time analysis (RTA) was used to perform base calling, and CASAVA (version 1.8.2) was used for converting base call files (.BCL) to FASTQ format and also to perform sequence adaptor trimming. Reads were then mapped to the mouse reference genome (mm10) using STAR (https://github.com/alexdobin/STAR), using default parameters. Counts tables were generated from aligned reads with HTSeq version 0.6.1. Statistical analysis was performed in R version 3.5.0. A matrix of read counts in all genes across samples was created from each samples' individual count data and pre-processing included removal of genes with zero expression across all samples. Differentially expressed genes were identified using the DESeq2 package version 1.22.2. Significantly expressed genes were thresholded using an adjusted p value of 1e-4 and a fold change of ± 2.

Single molecule FISH combined with immunofluorescence

Mice were quickly perfused in ice-cold PBS and the lumbar spinal cord dissected out and post-fixed in 4% PFA for 18 h. After 2 washes in ice cold PBS, tissues were subjected to sucrose gradient (10%, 20%, 30%) and subsequently embedded in OCT. A freezing microtome was used to collect 15 μm transverse section onto Superfrost Plus Micro Slides (VWR, Radnor, PA) and slides were stored at −80°C until use. For smFISH the RNA scope kit v2 was used (Advanced Cell Diagnostic, ACD 323100). The experimental conditions were optimized using Positive Control Probes (catalog number 320881) and Negative Control Probes (catalog number 320871). For detection of mRNAs of interest, catalog probes against mouse IRF7, USP18 and Lgals3 (catalog numbers 534541-C3, 524651 and 461471-C2) were used. We followed the manufacturer's protocol, except for Protease III treatment, which was optimized to 22 min for better results in the downstream immunofluorescence application. Each probe was conjugated to

Opal-570 dye (Akoya, FP1488001KT). Subsequent immunofluorescent staining with antibodies against Iba1 (Abcam ab5076, 1:200) or GFAP (Abcam ab4674, 1:500) was performed overnight at 4°C in PBS 0.05%Triton supplemented with 5% Donkey serum. Secondary antibodies (1:500) and Nissl stain (1:500) were incubated at Room temperature for 4 h. Slides were mounted using Prolong gold antifade mountant with DAPI (Thermo Fisher, P36931) and imaged using a 20x objective. RNA molecules in each cell type were counted by an observer blind to genotype in 50 cells (per each cell type) per mouse.

QUANTIFICATION AND STATISTICAL ANALYSIS

The statistical tests used in this study are indicated in the respective figure legends. In general, data with single independent experiments were analyzed by Student unpaired t test to determine statistically significant effects ($p < 0.05$). Data with multiple independent experiments were analyzed by one-way ANOVA to determine statistically significant effects ($p < 0.05$).

DATA AND CODE AVAILABILITY

The data discussed in this work have been deposited in NCBI's Gene Expression Omnibus under accession number GEO: GSE146141.